NTNU – Trondheim
Norwegian University of
Science and Technology

Fatigue properties of adhesive joints in composite patch repair

Audun Reinsborg Log

Mechanical Engineering
Submission date: June 2012
Supervisor: Andreas Echtermeyer, IPM

Norwegian University of Science and Technology
Department of Engineering Design and Materials

Norwegian University of Science and Technology

TMM4511 MASTER THESIS

FATIGUE PROPERTIES OF ADHESIVE JOINTS IN PATCH REPAIRS

Author:
Audun Reinsborg Log

Supervisor:
Andreas Echtermeyer

THE NORWEGIAN UNIVERSITY
OF SCIENCE AND TECHNOLOGY
DEPARTMENT OF ENGINEERING DESIGN
AND MATERIALS

MASTER THESIS SPRING 2012
FOR
STUD.TECHN.
AUDUN REINSBORG LOG

FATIGUE PROPERTIES OF ADHESIVE JOINTS IN PATCH REPAIRS
Utmattings egenskaper av lim forbindelse i lapp reparasjoner

The Co-Patch project is developing a novel, effective method for repair and/or reinforcement of cracks or corroded areas on steel structures. The repair can be done without hot work resulting in big savings in areas with fire hazard. The technology is based on bonding composites patches across the damaged steel.
This thesis shall test and model fatigue behavior of the adhesive joint between metal and composite.

The thesis should include the signed problem text, and be written as a research report with summary both in English and Norwegian, conclusion, literature references, table of contents, etc. During preparation of the text, the candidate should make efforts to create a well arranged and well written report. To ease the evaluation of the thesis, it is important to cross-reference text, tables and figures. For evaluation of the work a thorough discussion of results is appreciated.

Three weeks after start of the thesis work, an A3 sheet illustrating the work is to be handed in. A template for this presentation is available on the IPM's web site under the menu "Undervisning". This sheet should be updated when the Master's thesis is submitted.

The thesis shall be submitted electronically via DAIM, NTNU's system for Digital Archiving and Submission of Master's thesis.

Torgeir Welo
Head of Division

Andreas Echtermeyer
Professor/Supervisor

Acknowledgements

This is a master thesis written in the spring semester of 2012 on the fatigue properties of adhesive joints. I wanted to write on a subject that included analysis work, advanced materials, lab work and would have a large impact. Patching steel structures is a creative idea and the benefits are obvious when looking at the alternatives.

The work on this thesis has put me to a lot of different challenges such as composite production, developing test rigs, setting up data acquisition, script writing for data reduction and analysing parameters and methods in simulations. It has been a learning process from which I have gained considerable amounts of valuable experience.

I would like to thank my supervisor Andreas Echtermeyer for good help in discussing issues encountered on the way. I also would like to extend my gratitude to Halvard Støwer for help in setting up the test machines and data acquisition equipment, Stanislav Schechebetov for help with simulation and test analysis and Jon Harald Grave for help in creating the test specimens.

Abstract

This paper is a master thesis written at NTNU for the Co-Patch project. The Co-Patch project is an EU-funded consortium of 15 organizations from 8 different countries, developing a standard for composite patch repair of steel structures in fire hazard areas. The standard includes methods for dimensioning against delamination. This thesis looks at the fatigue properties in delamination of patches from their substrates.

By testing Double Cantilever Beam and End-Notched Flexure specimens in fatigue loading, G-N curves were made for Mode I and Mode II fatigue fracture. This gives an indication of the lifetime of a patch given a specific cyclic load condition and a pre-existing crack. The longest cycle life recorded was 4.35E5 cycles at 104 J/m^2 for Mode I and 1.23E5 cycles at 122 J/m^2 for Mode II.

Furthermore, a relation for crack propagation rate and energy release rate in Mode I was found for low cycle life estimation. From this relation, the crack front position may be estimated for a given set of cycles through calculations using Paris' law. Based on the quasi-static data of a previous report, and the fatigue data found in this thesis, a numerical simulation procedure for crack propagation was proposed. Using direct cyclic fatigue analysis and Virtual Crack Closure Technique based on linear elastic fracture modelling, the crack propagation may be estimated for patches exposed to combined conditions, such as plane strain/plane stress and different fracture modes, as well as on advanced geometries.

Though the model and specimen showed a difference in stiffness, the procedure itself was validated as a viable way to estimate fatigue crack growth.

Sammendrag

Denne masteroppgaven er skrevet ved NTNU for Co-Patch-prosjektet. Co-Patch-prosjektet er et EU-finansiert konsortium av 15 organisasjoner fra 8 forskjellige land, som utvikler en standard for lapping av stålkonstruksjoner i brannfarlige områder ved bruk av kompositttmaterialer. Standarden skal inkludere fremgangsmåter for å dimensjonere reparasjonen mot delaminering. I denne oppgaven er det blitt sett på utmattingsegenskapene i grensesnittet mellom kompositt og stål .

Ved å teste limforbindelsen mellom stål og kompositt mot sykliske laster, er det blitt laget GN-kurver for sprekkinitiering i Modus I og Modus II. Dette vil bidra til å gi en indikasjon på levetiden til en patch gitt en bestemt syklisk belastningstilstand og en initiell sprekk. Den lengste levetiden som ble funnet var på 4.35E5 sykluser ved 104 J/m^2 for Mode I og 1.23E5 sykluser ved 122 J/m^2 for Mode II.

Videre ble en kurve for sprekkvekstrate i Mode I funnet for lavsyklusutmatting. Fra denne kurven, kan sprekkens posisjon anslås ved hjelp av Paris' lov. Basert på kvasi-statiske data fra en tidligere rapport, og utmattingsdata funnet i denne oppgaven, ble det foreslått en numerisk simuleringprosedyre for sprekkvekst. Gjennom bruk av Direct cyclic fatigue analysis og Virtual Crack Closure Technique basert på lineærelastisk bruddmodellering, kan sprekkveksten anslås for lappede konstruksjoner utsatt for kombinerte forhold som for eksempel plan spenning/plan tøyning og mixed mode bruddtilstand. Tross en forskjell i stivhet mellom modellen og prøven, ble prosedyren validert som en mulig metode.

Table of contents

List of figures

List of tables

Nomenclature

ENF	End notched flexure
DCB	Double cantilever beam
N_a	Cycles to failure
l_e	Element length
l_{cz}	Cohesive zone length
δ	Displacement
C	Compliance
P	Force applied
G_I	Strain energy release rate, mode I
G_{II}	Strain energy release rate, mode II
G_{III}	Strain energy release rate, mode III
G_C	Critical strain energy release rate
VCCT	Virtual crack closure
CZM	Cohesive zone modeling
LEFM	Linear elastic fracture mechanics
CTOD	Crack tip opening displacement
E_i	Young's modulus
υ	Poisson's ratio
t_s	Thickness steel
t_{cf}	Thickness carbon fiber
w	Specimen width
υ_f	Fiber volume fraction
FEA	Finite Element Analysis
DGC	DCB grit blasted, wet layup GFRP
EGC	ENF grit blasted, wet layup GFRP
G_{thresh}	Cut-off threshold energy release rate
G_{equivC}	Critical energy release rate, mixed mode
LCF	Low-cycle fatigue
K_i	Penalty stiffness, normal
t_i	Interface strength
S_i	Stress
δ_f	Separation failure

1 Introduction

The Co-Patch project is a European funded project on Composite Patch Repair for Marine and Civil Engineering Infrastructure Applications. It is collaboration between 15 organizations from eight European countries to develop a standard on patching cracks in metal constructions and reinforce components by the use of composite materials.

Benefits of using composite patch repairs:

- Low weight on added material
- High fatigue resistance compared to welded/bolted joints
- No added stress concentrations
- No hot work required allowing application in explosive environment
- Direct application after a simple surface preparation
- Can be completed fast

In the process of determining a standard procedure for patch repair, a method for dimensioning of patches based on simulation should be developed. The patches, placed on bridges, boats or FPSOs, will be exposed to the impact of wind, waves, unloading and loading. The patches should be dimensioned for the cyclic loads that occur due to the nature of these conditions.

In a project work done during fall 2011, a model for simulating delamination was proposed. As a continuation, a fatigue model for delamination is to be found through the proceedings of this master thesis.

Tests to map the fatigue behaviour are used to find relations for estimating crack propagation rate and crack onset for Mode I and Mode II fracture. The parameters will also be used in the development of a simulation procedure. The simulation will be compared and benchmarked to tested results.

2 Theory

To construct proper tests and find the parameters needed for a simulation, it is necessary to look at the mechanics of the adhesive delamination.

2.1 Adhesive work

Adhesives are substances used to join two components together. The components are often referred to as substrates or adherends. The adhesive should have the thermodynamic properties to form intimate contact with both adherends and to coalesce. Different physics used to explain the bonding have been tied to dispersion of van der Waal forces, chemical bonds, molecular inter-diffusion of similar materials, electrostatic attraction and mechanical adhering through interlocking the adhesive within crevices of the adherend surface. [1] To enhance the mechanical adhering, surface treatments, such as grit blasting, is used to remove weakly bonded layers and create larger pores for better mechanical interlocking.

The breaking of these bonds is done by exceeding the attraction force between the adherent and the adhesive. The energy released is known as the thermodynamic work of adhesion, measured in J/m^2. In larger systems, the energy measured will include dissipated energy through bulk and extrinsic deformations, yielding higher values than just the theoretical work of adhesion. This should be accounted for when testing.

2.2 Fracture mechanics

Delamination of the composite from the steel plate is recognized as an interlaminar fracture. As described by Dillard and Pocious [2], a fracture occurs if cohesive tractions in the adhesive interface are sufficiently large so as to induce nonlinear irreversible deformation. The tractions are provided by potential energy loss between atoms of adherend and adhesive as the atoms are separated. The reduction in this potential energy between two surfaces is equal to the total strain energy, dU. The energy released per crack increment is the material parameter energy release rate, G, which relates the total strain energy to the crack propagation, the *cohesive zone*, as described by Griffith [3].

$$G = \frac{dU}{da} \tag{1.1}$$

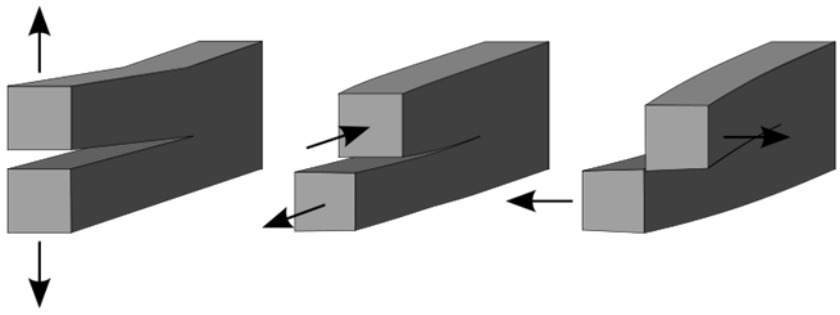

Figure 1 Mode I opening, Mode II out-of-plane shear and Mode III in-plane shear

The fracture mechanisms are divided into three separate modes: mode I opening, mode II out-of-plane shear and mode III in-plane shear. Crack propagation resistance for the different modes is described by G_I, G_{II} and G_{III} respectively. A typical method for calculating G is the area method explained by Carlsson and Pipes in [4] which calculates the area beneath the load curve registered for a crack propagation increment. However, this is best used to describe the energy lost in a full load cycle. An expression using compliance is deemed more effective for fatigue tests. [5]

2.3 Compliance relation

Total strain energy may be expressed as shown by Kinloch and Young [6] with the use of compliance and load.

$$U = \frac{1}{2} CP^2 \tag{1.2}$$

Critical value of $G = G_c$, at which point the material at the crack tip yields to the plastic strain, can be found by measuring critical load, P_c, at crack length a_c, when crack propagation occurs.

$$G_c = \frac{P_c^2}{2w} \frac{dC}{da} \quad , a = a_c \tag{1.3}$$

Provided a good estimate of the compliance curve, C (a), this can be used to measure the energy release rate at any given point during the fatigue tests. The compliance is recognized as a displacement-load relation, the inverse of the stiffness, and can be expressed by the equation

$$C = \frac{\delta}{P} \tag{1.4}$$

It is generally found by recording the difference in load over a certain displacement length in the elastic area of the load curve. This is highlighted in black in Figure 2.

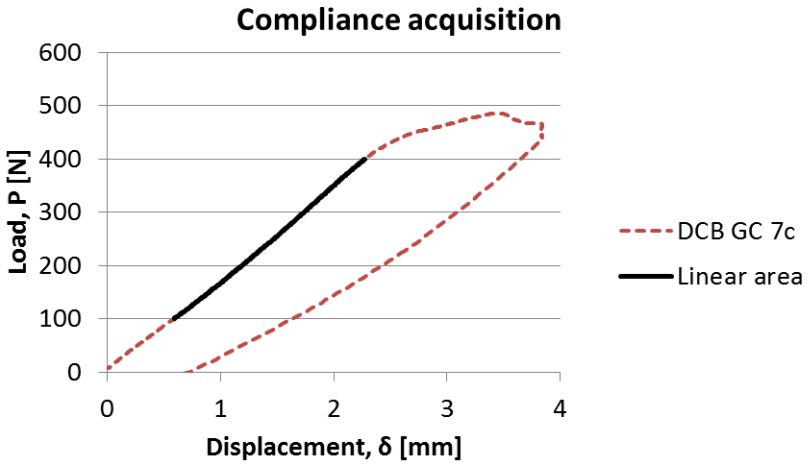

Figure 2 Compliance of a load curve found on linear elastic area

Geometries containing a crack will behave more compliant under loading than smooth geometries, and compliance will increase with crack length. Using this knowledge, an increase in crack length can be measured by a change in the compliance.

2.4 Fatigue theory

Fatigue is the degradation of cyclically loaded material. To find crack onset, a criteria frequently used and proposed by the ASTM fatigue standard [5], is the G-N curve, analogous to the SN-curve [7]. This relation provides an estimate for cycles to crack onset to the energy release rate by a power law

$$\Delta G = m_1 N_a^{m_2} \tag{1.5}$$

Where m1 and m2 are material parameters obstained experimentally ΔG is the effective energy release rate, $G_{max} - G_{min}$ and N_a is cycles to delamination onset. A widely used method for finding the relation between crack growth rate and energy release rate is through a power equation known as Paris' law of crack propagation [8]

$$\frac{da}{dN} = m_3 \Delta G^{m_4} \tag{1.6}$$

Where m_3 and m_4 are material constants obtained to fit experimental data and da/dN is the instantaneous crack propagation rate. This can be used to track the delamination growth and estimate the fatigue life of a patch. The analytical solution may prove complicated or very conservative, given that the energy release rate is geometry and load situation dependant and may change during crack propagation.

A numerical model that does the stress analysis along the interface and degrades the bond line in small increments is wanted.

2.5 DCB Tests

The double cantilever beam is a Mode I fracture specimen. The loads are introduced perpendicularly to the crack direction causing tensile stresses in the adhesive interface. The area method is more accurate and recommended practice [4] for finding the energy release rate in quasi-static tests when tests show no plasticity caused by extrinsic effects. Using area method in fatigue tests may prove difficult, and so compliance calibration method is used. For coherency with the quasi-static tests, the critical energy release rates from [9], found by compliance calculations, were used.

In combination with a relation between compliance and crack length, measures of compliance are used to find the crack length at arbitrary points of fatigue tests. To find an expression for the compliance, it is possible to use beam theory as done by Carlsson and Pipe [4]. Deflection in beams should by simple beam theory be proportional to the crack size, *a*, with the power of 3. This, however, assumes that the adherends are clamped or rigidly bonded at the adhesive front. Modified beam theory as presented by J.P. Berry [10] assumes the exponent may differ due to elasticity of the adhesive and should be found empirically.

The compliance calibration method also proposed by Berry [10] and supported by Benzeggagh & Kenane [11], assumes the exponent to be different from 3 with the relation

$$n = \frac{\Delta \log(C)}{\Delta \log(\mathrm{a})} \tag{1.7}$$

Using this expression for the compliance, the G_{IC} can be expressed as

$$G_{IC} = \frac{nP_c\delta_c}{2ba} \tag{1.8}$$

A Modified Compliance Calibration is also presented in the ASTM 5528 [12], but uses the total thickness of the specimen and hence it was not considered valid for a bi-material non-symmetric test. In a comparison [13], the compliance calibration comes out as being more conservative, but modified beam theory and modified compliance calibration are less flexible towards the use of asymmetric specimens.

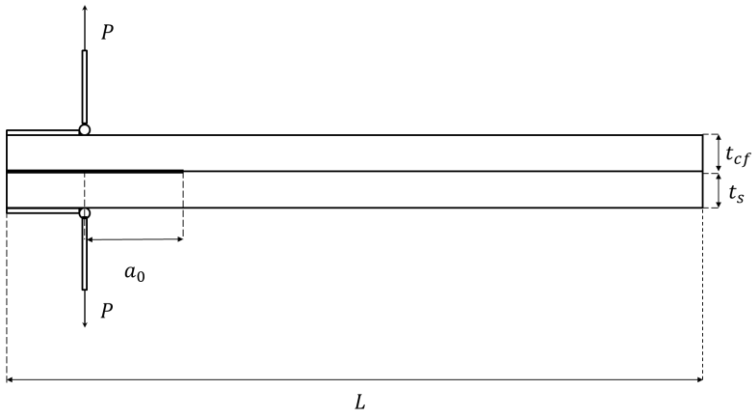

Figure 3: DCB test setup geometry

The loads were introduced using 1 mm thick piano hinges. They were fastened by a screw connection at the steel beam, and a screw-driven clamp at the composite patch beam. 5 mm thick steel plates were used as washers for added stiffness to the hinges. As crosshead movement was used for control and crack opening, the crack length was measured from the hinges.

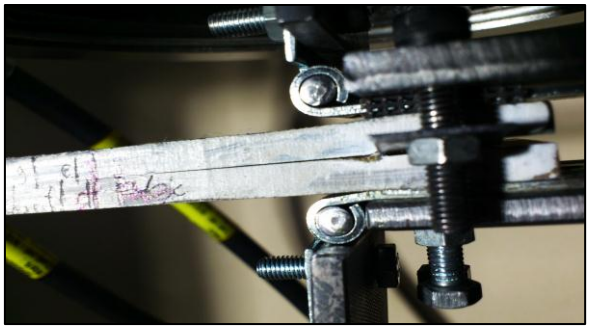

Figure 4: Hinge application

2.6 ENF Tests

The end-notched flexure specimen is a Mode II fracture specimen. It is a dual laminate specimen subjected to three point bending. When subjected to bending, the middle of the specimen will see pure shear stresses due to the tensile stresses directly above and the compressive stresses directly below the adhesive interface. Due to unstable crack propagation and the crack arresting at loading point [14], the area method is unfitting also for quasi-static tests. The best way to measure energy release rate is by the compliance calibration method, but with a different scheme than for DCB.

In similar tests conducted by Sinnerud [15] and Andresen and Echtermeyer [14], the compliance calibration for the ENF tests was made using an equation of the form

$$C = \alpha + \beta a^3 \tag{1.9}$$

Where constants α and β are found by curve fitting of test values. This was also supported in the standard recommendation by Davidson and Teller [16] as well as [17]. Using this in the equation for energy release rate (1.3)and we get the expression proposed by Russel and Street [18]

$$G_{IIc} = \frac{3P_c^2}{2w}\beta a^2 \frac{C}{\alpha + \beta a^3} \tag{1.10}$$

Here C is the measured compliance of the specimen with corresponding crack length. Strain energy release rate may then be calculated from the four parameters crack initiation load, P_c, displacement, δ, width w, and critical crack length a_c.

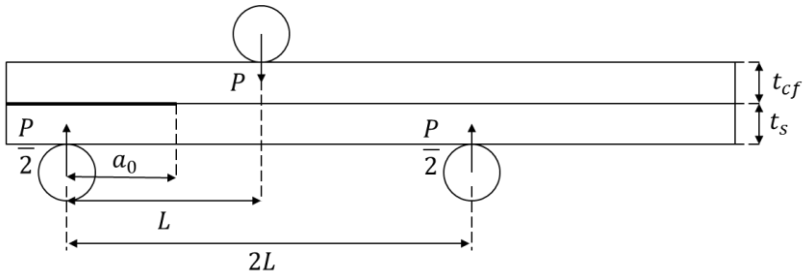

Figure 5: ENF test setup geometry

The specimens were placed on a two point rig with a total span, 2L, of120 mm as shown in Figure 5. The console was balanced, before the top load point was lowered onto the supported specimen using load control to find the zero position. Loads and displacements were controlled using crosshead sensors. All three loading points were supported cylinders with diameters of 10 mm.

3 Experimental procedure

Modes I and II will be tested. Mode III is also necessary for an accurate model, however, the analysis developed in chapter 4.6 may only use one set of fatigue parameters. The Mode III fractures are considered less relevant [15] and tests done by Li [17] indicate a normal behavior of longer fatigue life in Mode III compared to Mode II.

3.1 Specimen geometry

Geometry was selected according to ASTM standard requirements [12].Similar tests have been done previously by Sinnerud [15], Andresen and Echtermeyer [14] and specimen dimensions were chosen according to these, for the possibility of comparison. From the bottom, the specimens consist of one steel plate with a thickness, t_s, of 5 mm, one layer of $\pm 45°$ glass fiber composite with a thickness of 0.3-0.5 mm and 16 layers of unidirectional carbon fiber composite with a total thickness, t_{cf} of 4.8 mm. From the end of the specimen, a 50 mm long crack, a_0, was made using an insert of teflon tape to which the epoxy does not adhere. This was applied between the steel and the glass fibre/epoxy as this was shown to be the weakest interface in tests done by Andresen and Echtermeyer [14]. The width, w, was set to 25 mm. Each specimen was measured for thickness and width at three points along length to find the average values used in calculations.

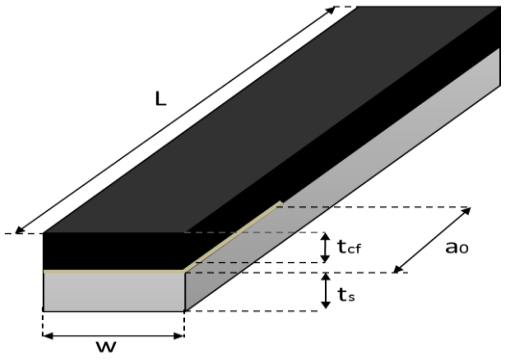

Specimen dimensions	[mm]
Length, L	240
Width, w	25
Thickness composite, td	4.8
Thickness steel, ts	5
Initial crack length, a0	50

Figure 6 Specimen geometry and dimensions

3.2 Specimen production

Steel plates were wiped with a cloth of acetone. It was then sent to grit blasting, using steel grit for a surface roughness according to SA2 ½ of 50 µm <Rz < 85 µm in accordance with Norsok 501 [19]. This was verified using an Elcometer 224. The crack insert was then applied in the form of a 30µm thick Polytetrafluoroethylene (PTFE) tape. The plates were wiped with acetone as described in ISO 8501 [20] less than 15 minutes prior to epoxy and glass fiber. One layer of $\pm 45°$ stitched glass fiber was applied and soaked with epoxy system ESR/ESH using a brush. Application was done at 21°C and 37% humidity. The epoxy was cured under vacuum, with peel ply, release film and breather at room temperature for 24 hours. Subsequently, 16 layers of unidirectional carbon fiber Toray M46JB pre-impregnated with resin system SE84LV from Gurit, was applied and cured under vacuum at 80°C for 10 hours as specified in [22]. Specimens were cut to specified geometry using a water jet at Asbjørn Krogstad AS. The sides of the specimens were painted with white correction fluid to spot the delamination front.

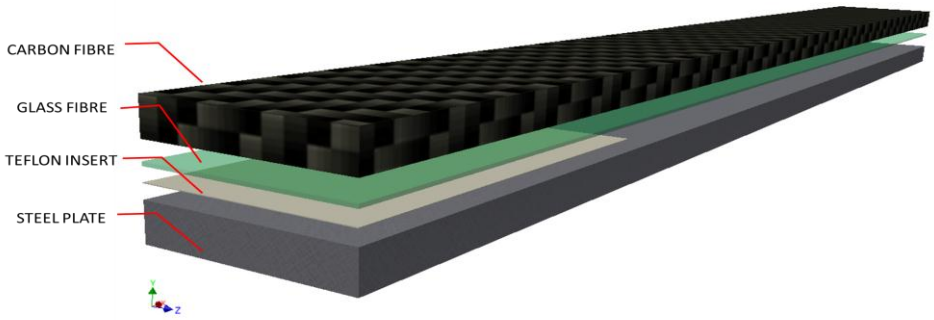

Figure 7: Layup for specimen production

8 ENF fatigue specimens and 8 DCB fatigue specimens were produced. They were made in the same batch as the quasi-static specimens tested earlier and listed in A.2.

3.3 Quasi-static testing

From quasi-static tests conducted earlier [9], critical energy release rate was found for Mode I and Mode II using the area method and the compliance calibration method. The tests were done using similar specimens at a crosshead rate of 2 mm/min. Parameters and procedure followed the standard ASTM 5528 [12] for DCB tests and the recommendations by Davidson and Teller [16] for ENF tests. The compliances recorded for relevant crack lengths were used in the cyclic tests and is listed with the critical energy release rates in A.3 and A.4. The values found were used for dimensioning of the load intervals in the fatigue testing.

3.4 Fatigue testing

The ASTM standard for DCB fatigue tests [5] recommends that the specimens are the same as for quasi-static tests. Furthermore, the specimens should be cycled between a minimum and maximum displacement $\delta_{min}$and δ_{max}. At onset of delamination growth, the number of displacement cycles N_a is recorded. Onset is determined, either by 5% increase in compliance, which is approximately 5% decrease in load, or by visual observation of crack propagation. Whichever occurs first. It was recommended to do the first test at $G_{Imax} = 50\%G_{Ic}$. This can be obtained from $\frac{\delta^2_{\max}}{[\delta_c]^2_{av}} = \frac{G_{Imax}}{G_{IC}} = 0.5$ where $[\delta_c]_{av}$ is the average value determined from quasi-static tests. Similarly, for load controlled tests, the wanted load values may be found using $\frac{P^2_{\max}}{[P_c]^2_{av}} = \frac{G_{Imax}}{G_{IC}}$.

Fatigue testing was done with the same constraints, and test geometry as the quasi-static tests. Recommended frequency values are between 1 Hz – 10 Hz. Most specimens were tested at a sinusoidal frequency of 1 Hz as per ASTM D6115 [5]. The longer lasting specimens were tested at a frequency of 4Hz. A full list of specimens is found in A.6. This is still well below the maximum test speed set in the standard. Testing of load rates' on critical energy release rate done by Gillespie et al. [23] showed that G_{II} decreased while G_I remained the same, and so a higher frequency is assumed to yield shorter fatigue life and is considered a conservative estimate. To measure the crack size, a method used by [24], [25] and supported by the standard is to measure the relation between crack size and compliance for the equally produced quasi-static specimens and

then measure compliance on fatigue loading curves to find the crack size at any given time.

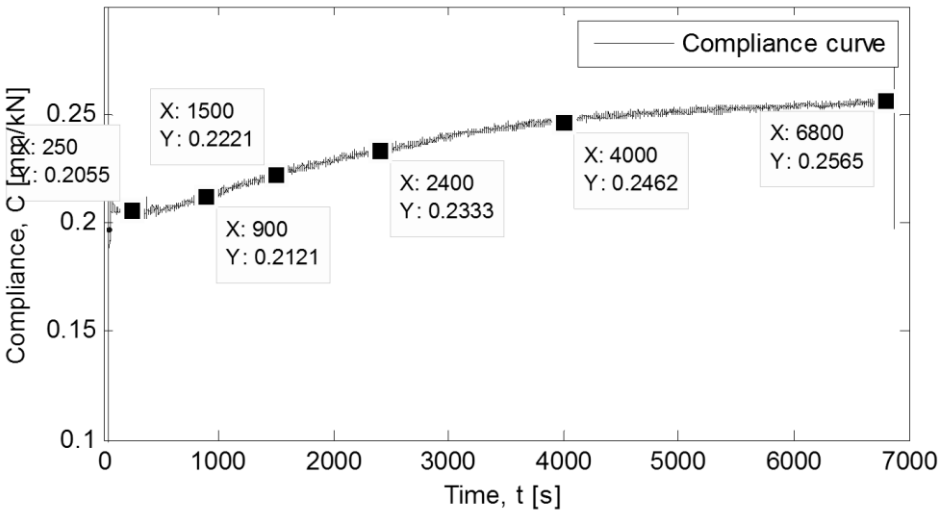

Figure 8: Compliance curve for EGC-C 5b

An example of the compliance history is shown in Figure 8. Points of 5% increase in compliance were found manually. Similarly, the maximum and minimum loads and displacements corresponding to the crack onsets were extracted from their respective plots.

3.4.1 Load control

It was determined that load control best represented the relevant load scenarios. Because the critical load, P_c, decreases with crack size, a load controlled test could prove unstable due to load amplitude exceeding critical load. It is important to keep load lower than the lowest recorded critical load for the tested crack size span, $P_a < P_{Cmin}$. Specimens EGC-C 1-5 were tested using load control.

3.4.2 Displacement control

Displacement control assures a stable fracture, as the energy release rate decreases when the crack propagates, causing the propagation rate to slow down. For displacement controlled tests, specimens were aligned and clamped into the rig. Subsequently, the zero load positions were found using load control before changing back to displacement control.

3.4.3 Data reduction

Load and displacement was recorded at 50Hz for tests of 1Hz and 200Hz for test speeds of 4Hz. When crack onset was observed, the loading was paused, the new crack length was marked with a 0.2 mm felt tip pen and a new data acquisition was started. Because of external data acquisition, energy release rates were calculated after testing using data reduction schemes described in 2.5 and 2.6. The load curves, displacement curves and the compliance curves were plotted for each test increment, using a script as described in A.1. The maximum load P_{max}, maximum displacement, $\delta_{max,}$ cycles to failure, N_a, and compliance, C, were extracted from the plots and used in equations (1.8) and (1.10) for calculations of tested G_{max} and ΔG. The ΔG was plotted against da/dN and N_a in a

logarithmic chart and a linear fit was done to find the constants of equations (1.5) and (1.6). The curve fits and parameter acquisition procedure is found in A.8

3.5 Equipment

An Instron 100kN was used for the testing with an HBM Spider8 and Catman for data acquisition. Maximum test loads should not be lower than 10% of maximum of the load cell [5]. If the loads are lower the ASTM Standard allows for a smaller load cell to be applied in series. An AEP TCE load cell of maximum load 1t was applied in series. Because of crosshead displacement range of $\pm 127{,}5\,mm$, a 20 *mm* HBM LVDT was used to accurately measure displacement. The load cell was calibrated using an already calibrated load cell and the LVDT with a calibration device for extensometers. The final setup for DCB testing is shown in Figure 9.

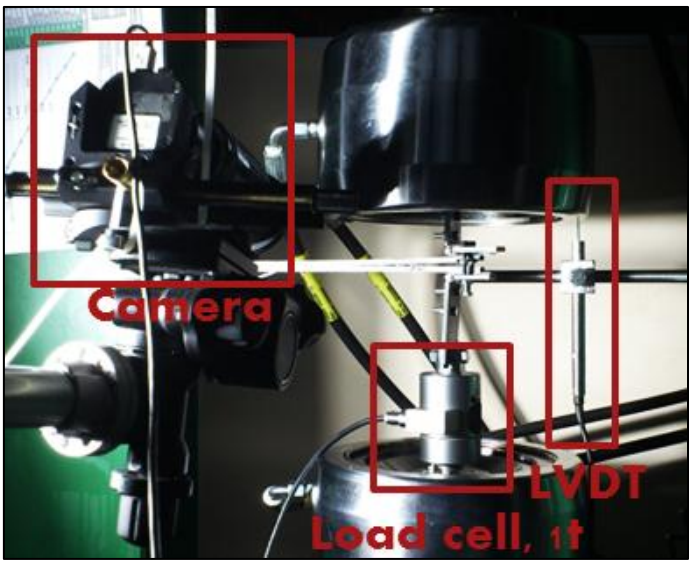

Figure 9 Equipment setup DCB testing

For the ENF tests, permitted loads were generally higher, and an Instron 50kN was used. The setup was aligned prior to and after insertion and is shown in Figure 10

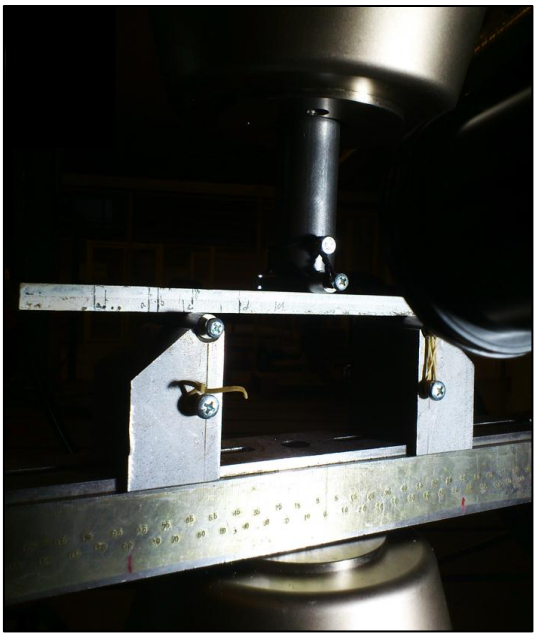

Figure 10 ENF Test setup

An SMX 150-M camera with a tele-lens in combination with a Hedler DX15 halogen lamp was used to spot the crack on the mounted specimens during testing. For the ambiguous cases, a handheld light microscope was used.

3.6 Measuring crack length

Measuring the crack lengths during testing is a highly operator dependent problem and as such a considerable source of error. An article by Davidson and Teller points out that measurements done visually may differ by several millimeters and may cause a difference in measured strain release rate of up to ~ 70% [16]. A study made by Vinciquerra and Davidson sees that different operators may measure crack lengths with an error of 30% [26]. They suggested calculating the crack length from compliance-crack length relation. This is a possibility as long as a well-defined relation between crack and compliance is found. Before starting a test, the crack length may be calculated from the loading curve. After a finished test, the end crack length may be calculated from the unloading curve. Crack length may also be calculated during cyclic loading. To achieve this, a three point compliance calibration was done for each crack length tested. It was loaded at $\pm 10\ mm$ from tested crack length, and at the tested crack length [16].

Due to problems with the ENF tests discussed in 6.1.1, in the end, the cracks were still determined visually. If the load curve during testing showed a significant compliance increase without a new crack front being available, the specimen was stopped and unloaded. It was then loaded until critical load when crack propagates to the loading point. The new crack front was marked and if non-ambiguous, the new crack was used for another fatigue increment. The compliance curves were only used as a measure of when the crack length had increased.

An attempt was made using B-scan with the Olympus 38DL Plus, but showed few results due to the device only being calibrated for one material, showing delamination along the whole specimen.

4 Results

4.1 Compliance calibration validation

A problem occurred with the ENF tests in which compliances during cyclic tests did not compare to compliances recorded from the three point calibrations.

A test was made to see if loading speed or loading interval had an effect. A specimen was loaded at speeds from between 2 and 60mm/min with increments of 5mm/min. Subsequently, compliance was extracted for the different speeds and different load intervals. 1.3 kN was the absolute maximum value in the calibrations, 0.5 kN was the lowest maximum load. Loads were always extracted above 0.2 kN to eliminate initial extrinsic effects

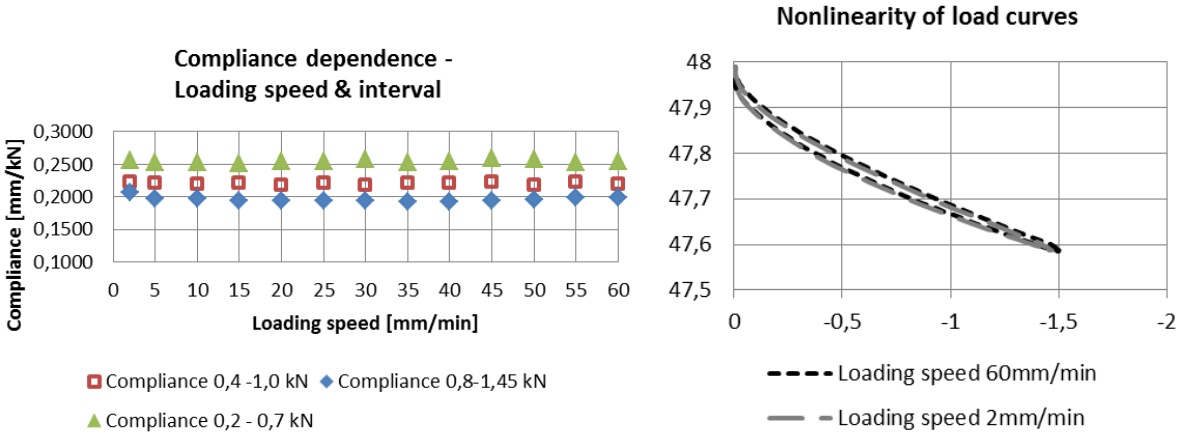

Figure 11 Relation between compliance and loading speed and load interval

No apparent dependency was shown for loading speeds between 2 – 60 mm/min. A clear dependency between load interval and compliance was seen. This is apparent when considering the nonlinearity present in the load curves. The compliance must thus be measured at the load interval relevant to the cyclic test.

Tests done using a sample of calibrations, shows the results of extracting compliance from different intervals on the load curve. A change in the calibration constant β will directly result in a change in energy release rate. The variance in calibration constants depending on where the linearization has been performed on the load curve is a valid source of error.

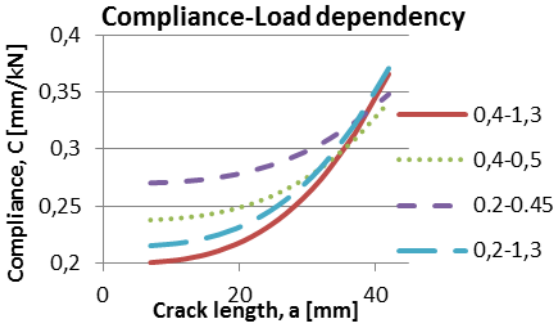

P interval	β	β/βfull
0,2-0,4	1,05E-06	0,50
0,2-1,3	2,11E-06	1,00
0,4-1,3	2,24E-06	1,06
0,4-0,5	1,40E-06	0,66

Figure 12: Effect of compliance calibration constant β

The maximum deviation was recorded to be 50%. Due to the equation for energy release rates, this directly translates to a 50% increase in calculated energy release rate. The compliance curve is a significant source of error. Because the ENF calibrations could not be done at higher loads without going to fracture, the compliance calibration parameters from the quasi-static tests were used.

Also for the DCB tests, compliance from the quasi static tests was used to calculate the necessary applied load for the wanted G-values in each test.

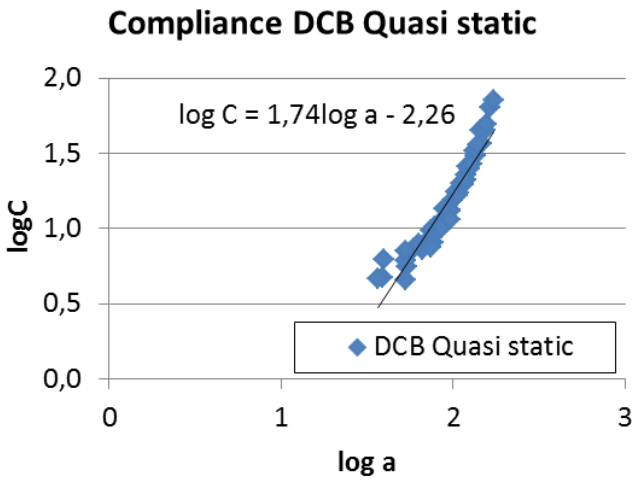

Figure 13: Compliance calibration from quasi static tests, DCB

For the final calculations of tested G-values, a validation was made to see if the crack lengths calculated from the quasi static specimens followed the visual recordings of the crack. The difference is plotted in Figure 14. A new calibration was done using the values of the specimen DGC-C 2 which was cracked incrementally until the end of the specimen.

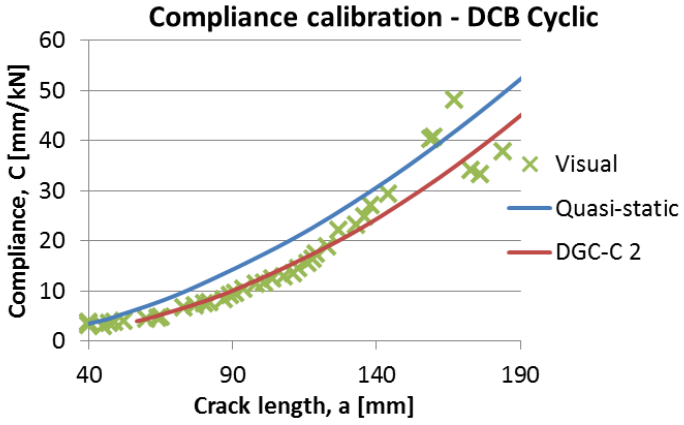

Figure 14: Compliance calibration for fatigue tests

The quasi-static calibration was deemed fit, it had more measurements and was used in the quasi static estimate of G_{IC}. It was thus used for the final calculations. Because of deviations between recorded compliance and visually recorded crack length when crack length exceeded 140 mm, no results after a crack length of 140 mm was used.

4.2 DCB Results

From the DCB tests, the resulting Paris curve and G-N curves are plotted in figures Figure 15 and Figure 16. All results are listed in A.6.

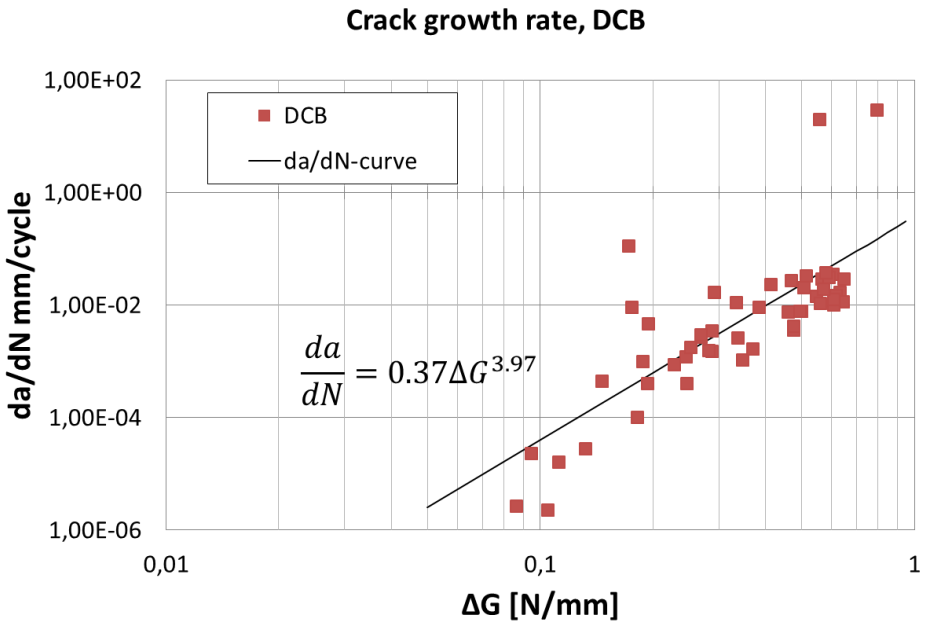

Figure 15: Paris' regime, DCB

The maximum load was DGC-C 5a which fractured instantly at ΔG=794 J/m^2. The lowest value tested was ΔG = 86 J/m^2 which was stopped, without propagation, at 236 000 cycles. The highest number of cycles was DGC-C 6e with 436 000 cycles at ΔG=105 J/m^2.

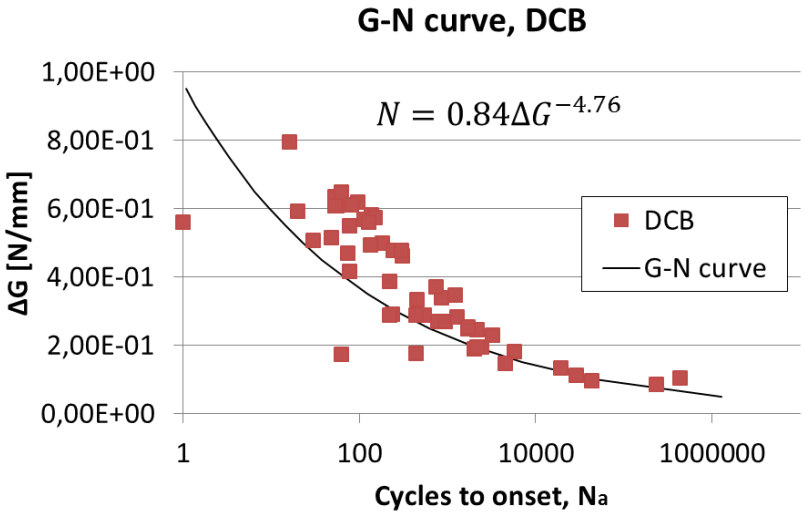

Figure 16: G-N curve, DCB

For both specimens tested with displacement control at 4 Hz and 1Hz we see a similar behavior in the decrease in crack growth rate for each increment.

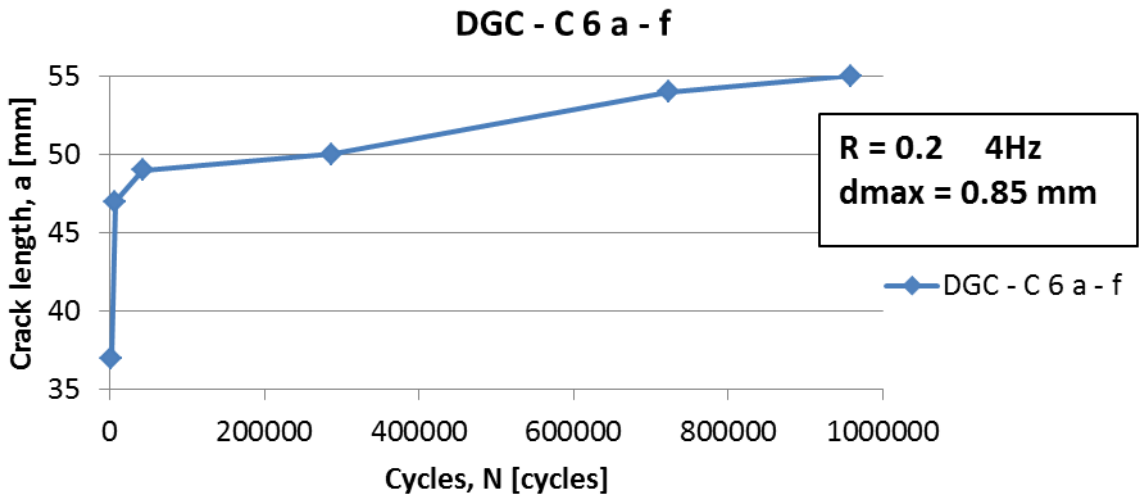

Figure 17: DCB crack growth at 4Hz, high cycle

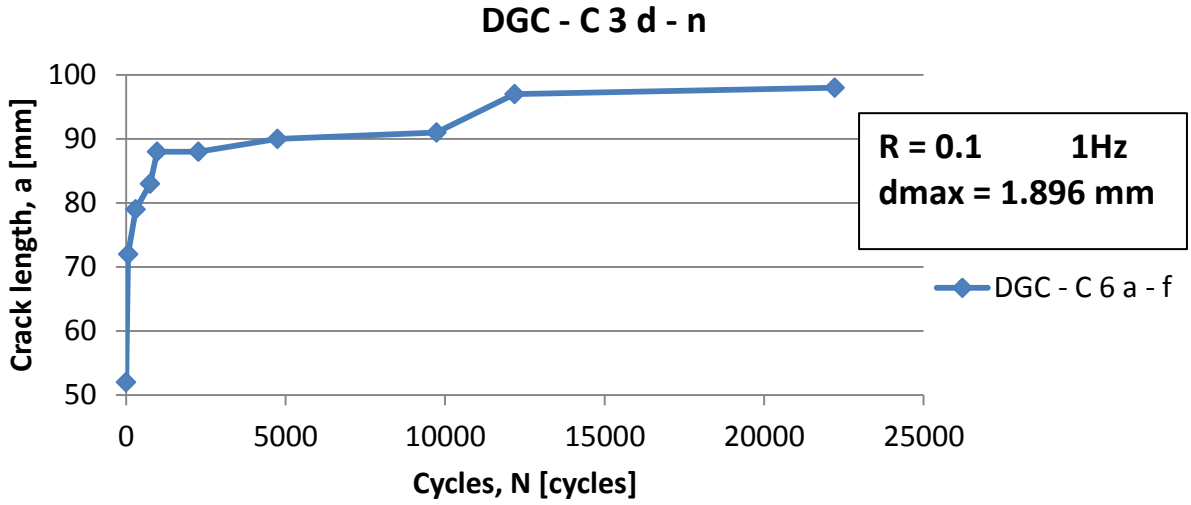

Figure 18: DCB crack growth at 1Hz, low cycle

4.3 ENF Results

From the ENF tests, a G-N curve was created. No specimen achieved run out. The lowest load tested was specimen EGC-C 3a which lasted 2 500 cycles at ΔG=105 J/m^2. The highest load was EGC-C 2a which lasted 182 cycles at 786 J/m^2.

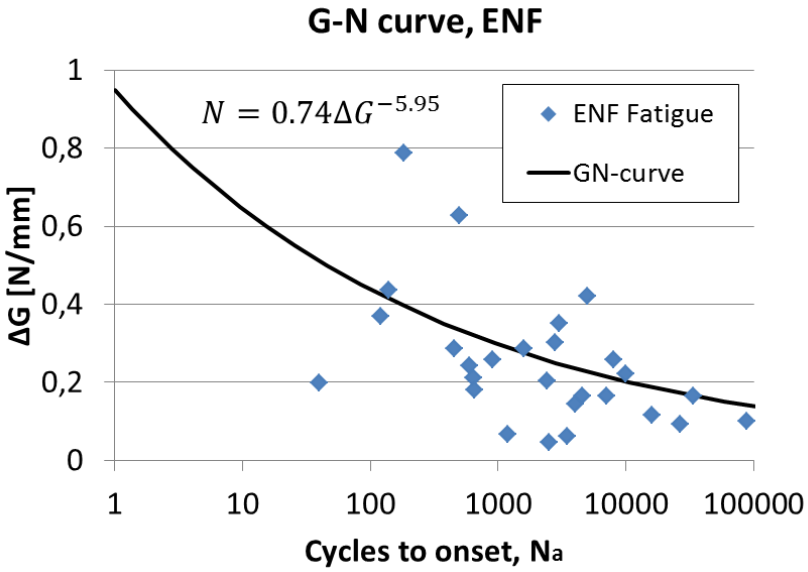

Figure 19: G-N curve, ENF

The G-N curve indicates a higher critical load than the one obtained through quasi-static testing.

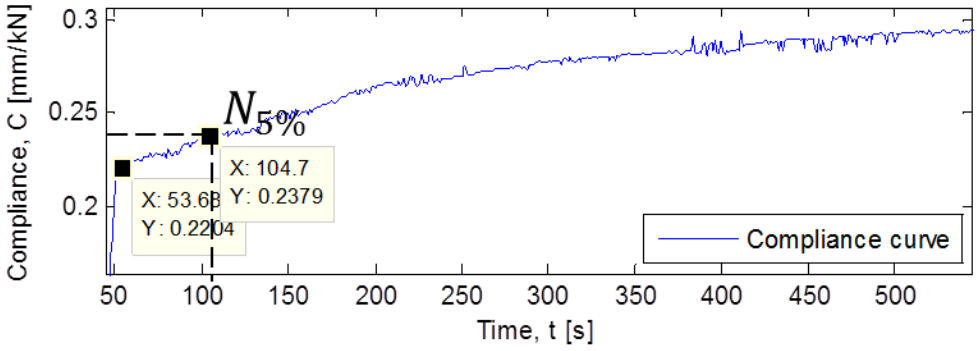

Figure 20: Compliance curve, displacement control, EGC-C 1c

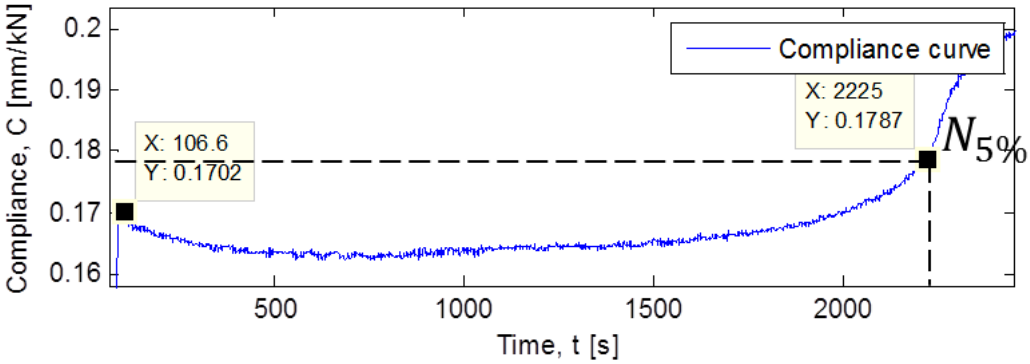

Figure 21: Compliance curve, load control, EGC-C 7a

Compliance growth for the displacement controlled test stagnates with increasing compliance. The load controlled test grows exponentially until crack is arrested at load point.

4.4 Comparison

A comparison of fatigue life between specimens subjected to Mode I and Mode II load conditions is shown in Figure 22. More test results are available for DCB as they are less likely to achieve unstable propagation an may have more crack increments per specimen.

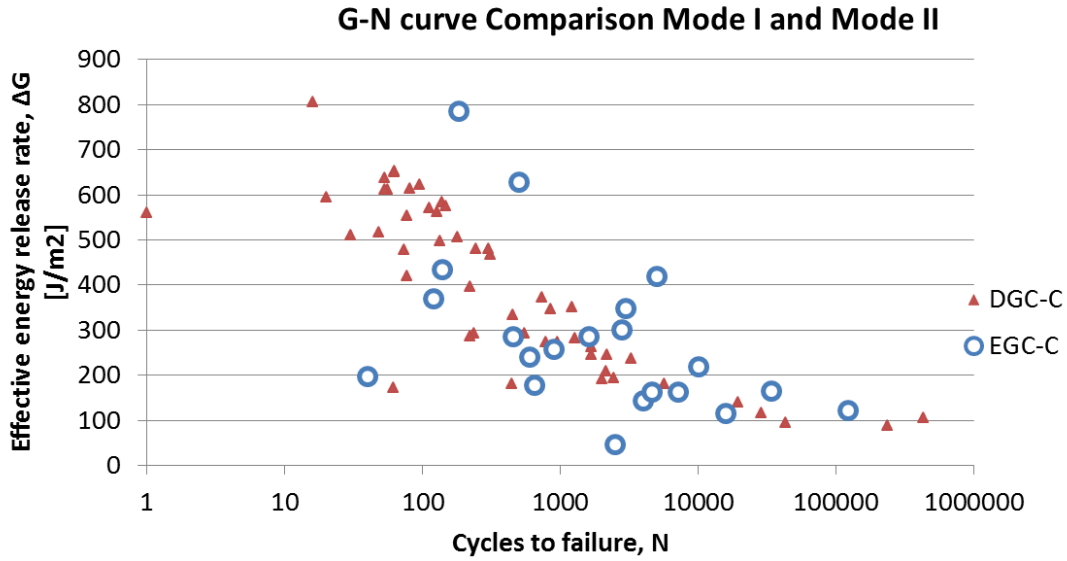

Figure 22: Comparison between Mode I and Mode II fatigue life results

We see that the fatigue life is similar for both modes though $G_{IIC} < G_{IC}$. The ENF also show more scatter than the DCB tests.

4.5 Material relaxation

When starting a fatigue test in ENF, it was noticed a trend where the compliance immediately increased significantly over the first cycles without there being any sign of crack propagation. It was proposed that the epoxy was subject to stress relaxation or creep. As an indicator of the effect of the stress relaxation, one specimen was loaded to a constant displacement for 20 minutes. After 20 minutes, the initial load was reduced from -0.62 kN to -0.54 kN. This translates to a load reduction, or compliance increase of 12%. A load reduction of 5% was achieved after 112 seconds.

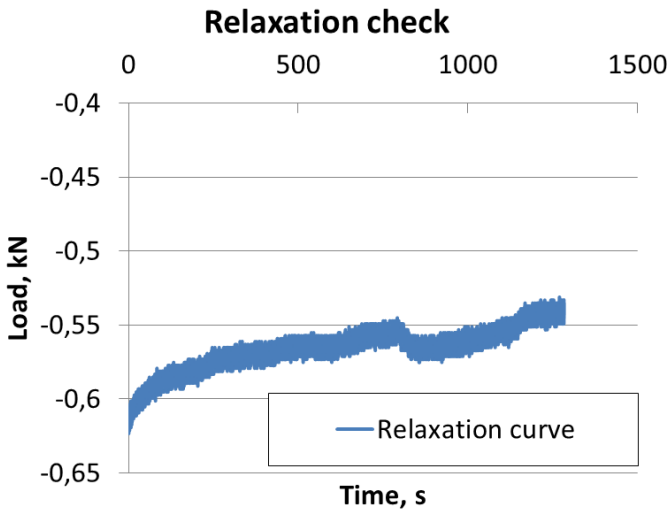

Figure 23: Load curve for creep test

Assuming stress relaxation occurs also at cyclic loading, this opens for the error of falsely assuming crack propagation when stress relaxation has occurred.

4.6 Fiber bridging

The test specimens were subject to bridging. This simulation does not apply, nor account for any stiffness altering effects at the cohesive zone. The effects were not strongly apparent, but in the compliances mapped for the specimen DCG-C 2 in Figure 14, the compliance did not follow a typical curve after approximately 140 mm.

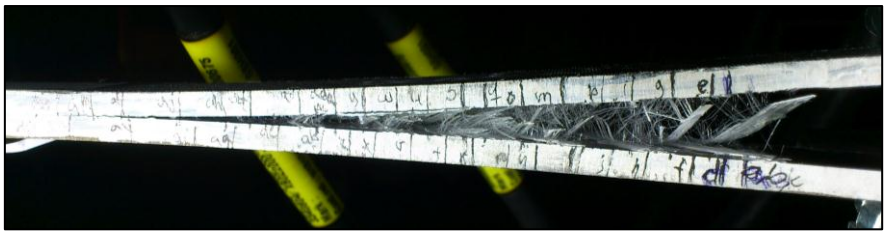

Figure 24: Fiber bridging on the specimen DGC-C 2.

5 Simulation procedure

No crack propagation simulation using cohesive elements was inherent in Abaqus for the cohesive zone model used in [9], and so a direct cyclic fatigue simulation is presented. This is based on VCCT, Virtual Crack Closure Technique, and uses the same initial conditions and cohesive zone interpretation.

5.1 Virtual Crack Closure Technique

VCCT uses theory of Crack tip opening displacement, CTOD. The interface is rigidly bonded when not cracked and the bond line thus does not contribute to compliance. It uses linear elastic fracture modelling, LEFM, to calculate crack propagation.

5.1.1 Fracture criterion

Energy release rate is calculated using equation (1.11) between the crack front and the closest nodes as shown in Figure 25. The loads at the bonded nodes depend on the substrate stiffness.

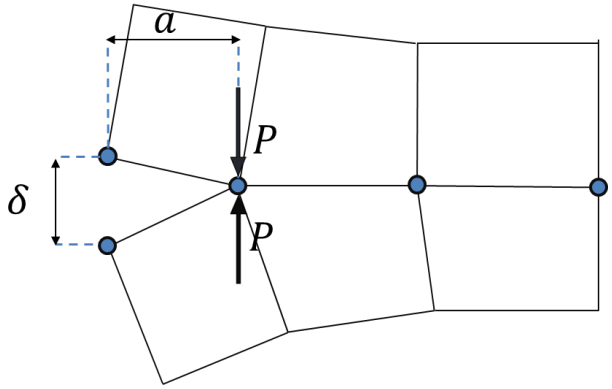

Figure 25: VCCT Crack propagation

The failure criterion used for the nodal bond connection is

$$\frac{P\delta}{2wa} = G_I > G_{IC} \tag{1.11}$$

Where P is the force between the connected nodes, δ is the displacement between the preceding released nodes and *a* is the distance between the released and connected nodes. If the calculated energy release rate exceeds critical energy release rate, the nodal contact is removed and the crack propagates one element length. The solid elemental length is thus directly proportional to the resolution of the crack propagation increments. For the criteria to work there must be a displacement between non-bonded nodes of master and slave surfaces, in addition to a connective force at the bonded region. Due to the nature of the criterion, degradation and crack fronts must be specified for onset to occur.

5.1.2 Damage evolution law

It is possible to choose between Reeder, power and BK law when calculating the total energy release rate. A comparison by Song [27] argues that the BK law renders more accurate results. BK law is the reduced form of Reeder law when $G_{IIC} = G_{IIIC}$ as was assumed at the start of this thesis.

$$G_{equivC} = G_{IC} + \left(G_{IIC} - G_{IC}\right)\left(\frac{G_{II} + G_{III}}{G_I + G_{II} + G_{III}}\right)^{\eta} \tag{1.12}$$

The BK-exponent η should be found experimentally by Mixed Mode specimens as described in [11] This was beyond the scope of this thesis and hence fatigue tests and validation may only be done correctly on specimens in pure mode I or mode II loading. The exponent was set to the default value of 2.284

The fracture criterion states that when the fracture factor, *f*, reaches a value of 1, the crack-tip node debonds

$$f = \frac{G_{equiv}}{G_{equivc}} \tag{1.13}$$

5.1.3 Convergence factors

The factor operates within a tolerance, f_{tol}, described in equation (1.14)- This is usually set to 0.2

$$1 \leq f \leq 1 + f_{tol} \tag{1.14}$$

In addition, viscosity coefficient is set to 0.1 to help overcome convergence difficulties for unstable crack propagation. For stabilization, step damping factor was set to 0.002 as is default. The criterion is implemented through the keywords listed in Figure 26.

```
*DEBOND, SLAVE=Slave, MASTER=Master

*Fracture Criterion, type=VCCT, mixed mode behavior=BK, normal
direction=MTS, viscosity=0.1
GIC, GIIC, GIIIC, η
```

Figure 26: Keywords, VCCT Fracture criterion

5.2 Low cycle fatigue simulation

The G-N curve may be used for calculating onset, and as dimensioning by making sure energy release rate does not exceed run out values. To calculate the life expectancy of a pre-cracked repair patch, the crack growth rates of different energy release rates may be plotted according to Paris' law. In a numerical simulation, the accuracy of energy release rates and the frequency of the recalculations may be adjusted.

5.2.1 Monotonic loading step

It is recommended to monotonically load the model to G_{max}. [28]. This is done in a static step, prior to the direct cyclic step with fatigue analysis.

5.2.2 Direct cyclic fatigue step

The first point is to create a direct cyclic fatigue step. Increment size is the inverse relation of numbers of increments per cycle. A fixed increment size of 0.1 gives 10 increments for each cycle. The cycle increment size is the amount of increments the damage is extrapolated forward. It is directly relevant for the resolution of the test. If a long lifetime is expected, large cycle increments may be chosen so as to not calculate damage for each cycle, which is computationally expensive, but rather get crack propagation state at specified times during the analysis. When dealing with large loads and short fatigue analysis, cyclic increments can be chosen down to a full resolution of minimum and maximum at 1. Maximum number of cycles determines the length of the analysis.

5.2.3 Fatigue criterion

Next a fatigue criterion must be implemented. From the Abaqus Documentation [29] we find that the criterion for onset of fatigue crack propagation is as follows:

$$f = \frac{N}{c_1 \Delta G^{c_2}} \geq 1.0 \tag{1.15}$$

Where N is cycles, c_1 and c_2 are material constants and ΔG is the effective energy release rate. If the criterion for onset is fulfilled, the crack propagation rate is calculated from the Paris' law

$$\frac{da}{dN} = c_3 \Delta G^{c_4} \tag{1.16}$$

The nodes will then be released to increase the crack length, a_N, over a set of cycles ΔN to an increased length $a_{N+\Delta N}$. The amount of nodes released is calculated from (1.16) and the known nodal spacing.

In total, the constants needed are:

- Material constants for initiation C1 and C2
- Material constants for delamination growth C3 and C4
- Total energy release rate power η
- Paris' limits $G_{thresh}, G_{equiv}, G_{pl}$
- Energy release rates G_I, G_{II}, G_{III}

The criterion is implemented through keywords as listed in Figure 27.

*DEBOND, SLAVE=Slave, MASTER=Master

*Fracture Criterion, type=Fatigue, mixed mode behavior=BK

c_1, c_2, c_3, c_4, G_{thresh}/G_{equivC}, G_{pl}/G_{equivC}, G_{IC}, G_{IIC},

G_{IIIC}, η, θ, f_v

Figure 27: Keywords, Fatigue fracture criterion

Benzeggagh and Kenane did the same mixed mode study on fatigue specimens concluding with the same correlation [30]. BK mixed mode propagation law is again used for the fatigue criteria.

To determine lower threshold we follow the highest tested value of G which goes to run-out, $N_D = 10^6$. The critical energy release rate, G_{equivC}, is found through quasi-static tests. Because the quasi static tests and fatigue tests were done in pure modes I and II, the BK equivalent energy release rate is reduced to the pure mode cases, ie.: $G_{equivC} = G_{IC}$ if all constants are obtained from the Mode I case. As the threshold values are not found, and the lowest value of G_{thresh}/G_{equivC} for DCB is lower than the equivalent tested for ENF, the Mode I case becomes dimensioning with a $G_{max}/G_{IC} = 0.095$. This is a high estimate, as the specimen did not in fact go to run out. The delamination growth and initiation parameters are found using by a linearized fit on areas shown in Figure 28 and Figure 29.

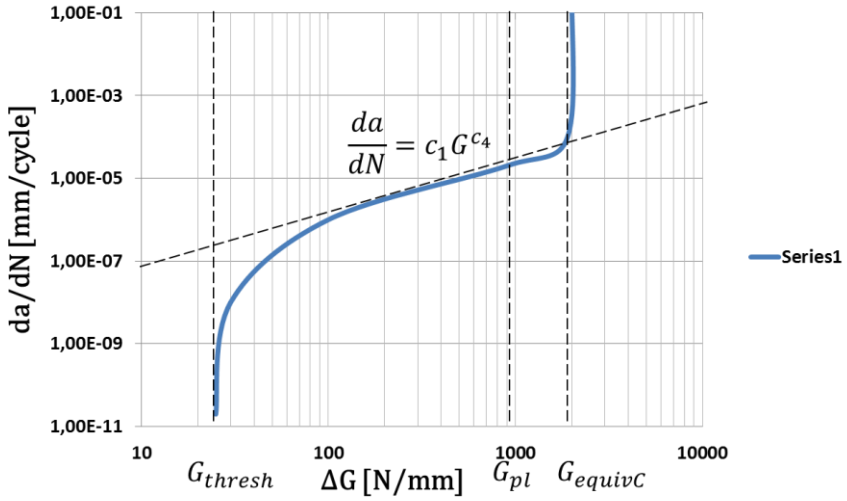

Figure 28: Crack propagation curve with Paris' regime

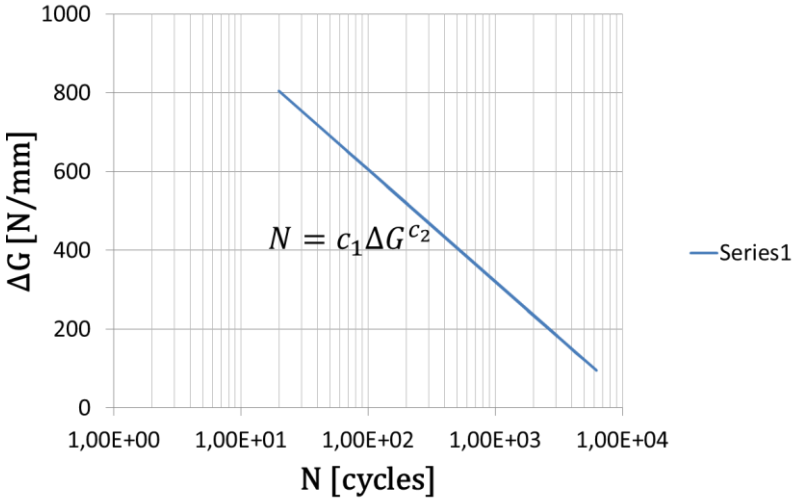

Figure 29: Fatigue life, G-N curve

From the results found in the experimental part, shown in Figure 15 and Figure 16, the material parameters needed for the fatigue simulation were extracted. The results are found in A.6 and A.7. Finally, the full table of parameters for the fatigue criterion is listed in Table 1.

Table 1: Parameters for Low Cycle Fatigue

Parameters Low cycle fatigue		
Gthresh/GequivC	0,095	
Gpl/GequivC	0,85	(default)
GIC	0,91	
GIIC	0,769	
GIIIC	0,769	
C1	0,840	
C2	-4,755	
C3	0,372	
C4	3,972	
η	2,284	(default)

5.2.4 Cyclic load application

The cyclic load is applied using periodic amplitude. It follows the Fourier series

$$a = A_0 + \sum_{n=1}^{N}\left[A_n \cos n\omega\left(t - t_0\right) + B_n \sin n\omega(t - t_0)\right] \tag{1.17}$$

It is set to start at max amplitude after quasi-static step. B_n and t_0 are set to zero.

*Amplitude, name=Amp-1, definition=PERIODIC
N, ω, t_0, A_0
A_1, B_1, A_2, B_2 …

Figure 30: Keywords amplitude

N is number of terms in the Fourier series, ω is the circular frequency in radiance per second, t_0 is the starting time and A_0 the constant term. A_1 is the first coefficient of the sine term, B_1 the first coefficient of the cosine term.

1 Hz yields 6.28 rad/s, t_0 For the analysis done, only A_1 is specified. A_0 is set to δ_{mean} and A_1 is set to δ_{amp}.

Tables listing all the parameters presented in this procedure are included in B.1

5.3 Material properties

5.3.1 Epoxy

The epoxy used in the glass fiber could be added to the model for more accurate simulation. Values gathered from datasheets [22] and [31]

Table 2: Adhesive values

[MPa]	E	υ	G
SE 84LV	3280	0.35*	1200
Epikote RIMR 135/RIMH 137	3200	0.35*	1185

*The υ was taken from [32]

5.3.2 Carbon fiber

The carbon fibers are Toray M46JB pre-impregnated with resin SE84LV from Gurit [22]. All plies are orientated 0° unidirectional to crack direction. Sinnerud [32] used the same resin, but the fibers were Grafil Pyrofil HS40 with elastic modulus of 455 GPa whereas Toray M46JB has 445 GPa. The tested values of the Pyrofil are used for modeling and the assumption that 16 plies provide almost equal stiffness to the 5 mm steel.

Table 3: Carbon fiber constants [32]

[GPa]	E_1	E_2	E_3	G_{12}	G_{13}	G_{23}	v_{12}	v_{13}	v_{23}
CF	222.3	15.87	15.87	4.3	4.3	3.4	0.2525	0.2525	0.5

5.3.3 Steel

To determine the strength and elastic modulus of the steel used in specimen production, it was tested using non-machined test specimens in transversal and longitudinal direction according to the procedure developed by Y. Zhang and M. K. Chryssanthopoulos for the Co-Patch project, based on the ASTM standard [33], including transversal strain gages for the poisson's ratio v_{12}. The values found are listed in Table 4. The longitudinal direction of the specimens is coherent with E_1. A synopsis is included in C.1.

Table 4: Steel values

[GPa]	E_1	E_2	v_{12}
Steel	219.3	205.2	0.3

5.4 Boundary conditions

Geometry is simplified under the assumption that no compliance is added from test rig. The loads are applied uniformly on the edges of the specimen by using a reference point

and a kinematic coupling. History outputs for displacement and load are also extracted from these points.

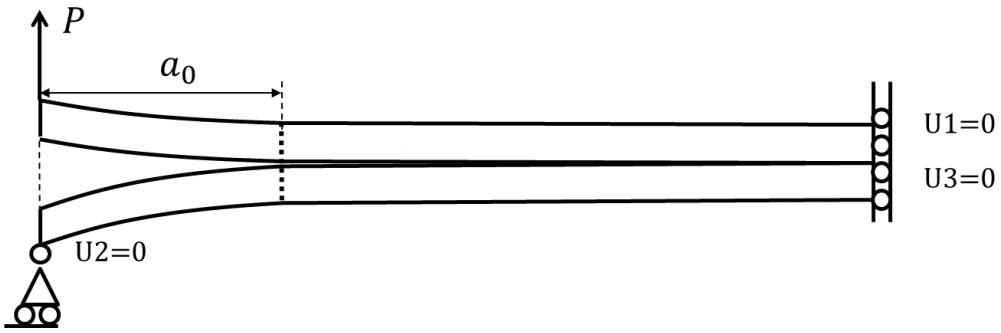

Figure 31: DCB Boundary conditions

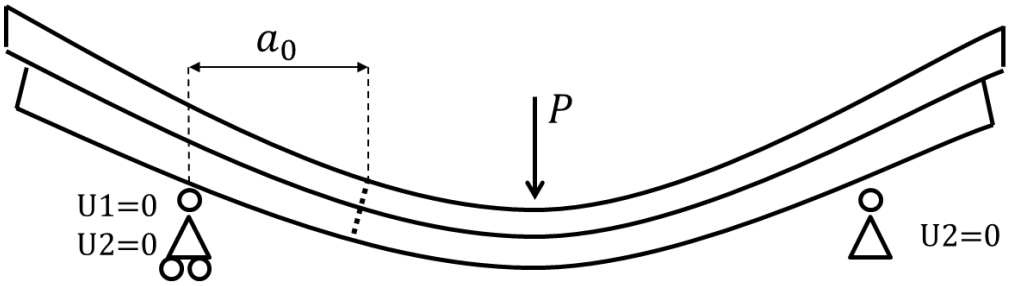

Figure 32: ENF Boundary conditions

The initial condition of surface-to-surface contact is selected for the entire bottom surface of the patch (master) as well as the entire top surface of the steel (slave). The bonding is limited to a predefined set of nodes including all slave nodes at the interface except where a crack opening is wanted.

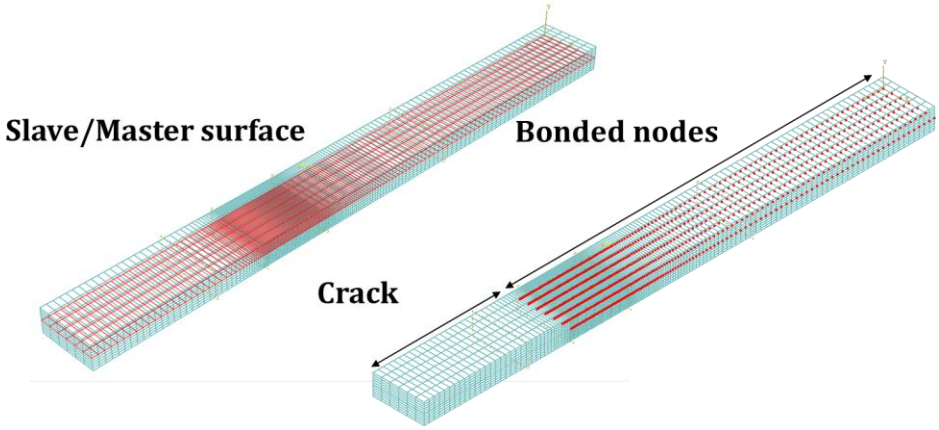

Figure 33: Surface contact and crack definition for VCCT

Due to the LEFM crack propagation explained, this method requires a pre-existing crack. If no crack is specified, no nodal displacement and no propagation is possible. However, these cracks can be placed at any point in the bonded surface and exposed areas should, under the assumption that there is no crack, nevertheless be modelled with a small set of unbounded nodes.

5.5 Element selection

Given that VCCT uses LEFM, only linear shell, brick or continuum shell element is possible. Simulations using linear solid element, C3D8R, have seen good results, and though continuum shell elements, SC8R, could with correct modelling be more computational efficient [34] [28], they have not been explored in this thesis.

5.5.1 Element sensitivity

A study of the element's effect on load response was done for ENF specimen. It was found that the stiffness increases with smaller element heights. No convergence was found, but an element height of 1.25 mm (4 elements through thickness, h) was considered an appropriate element size and was used in further testing. The stiffness decreased with shorter elements in longitudinal direction, but convergence was found at around 1 – 0.5 mm. 2.5 mm was used in further testing.

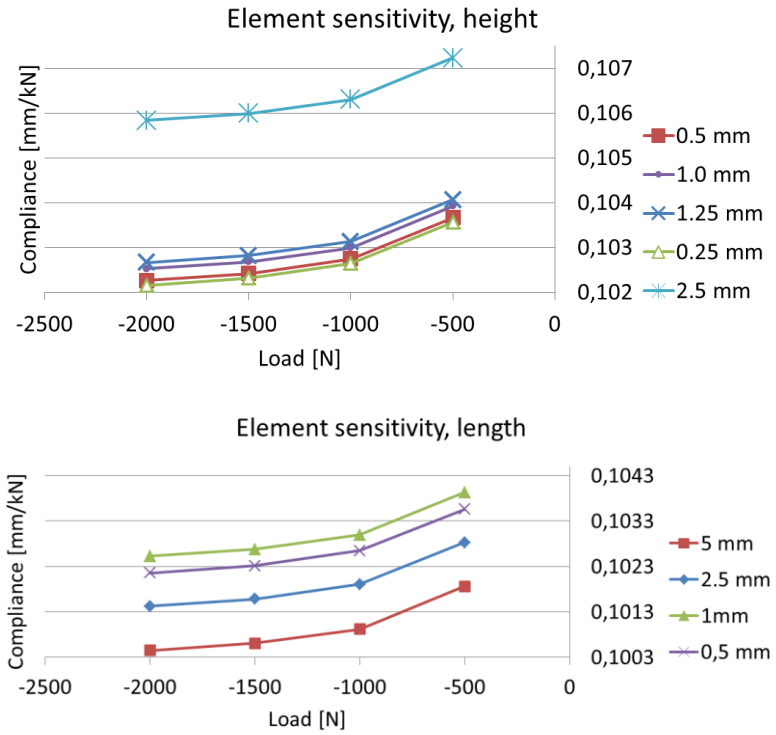

Figure 34: Compliances for different element heights and lengths, ENF

To see the effect of element length in fatigue analysis, tests are done using a cyclic displacement δ_{max} = 0.45 and δ_{min} = 0.048 on ENF with 5 elements in width and a decrease in element length at the crack front.

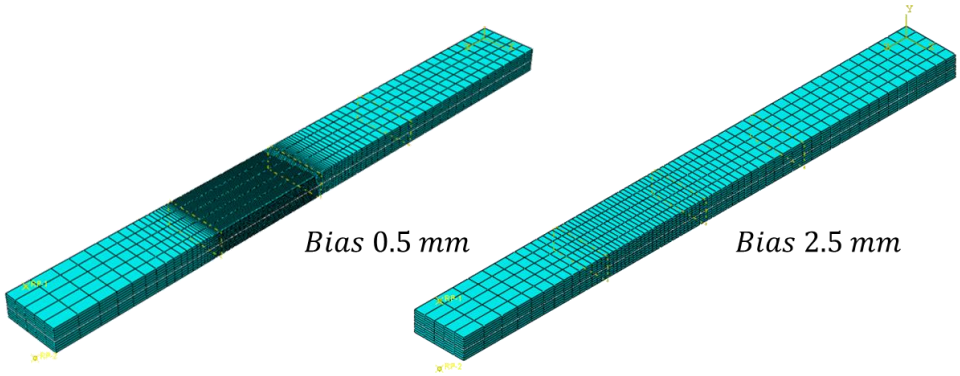

Figure 35: Meshing structure

There is complete overlap for biased and constant element length of 1 mm. The constant element length of 2.5 mm estimates an earlier and longer fracture. The element lengths of 1 mm and lower are computationally expensive, but elements should be smaller than 2.5 mm. Computational power can be saved without reducing quality by meshing a coarse mesh outside the bond.

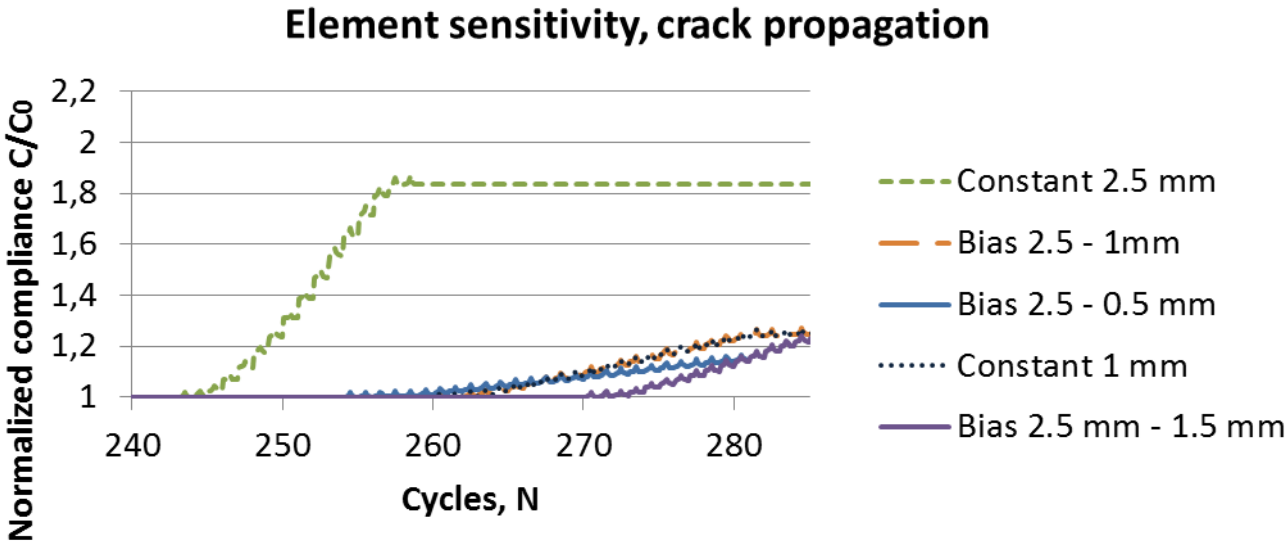

Figure 36: Element sensitivity, crack propagation of ENF

Figure 36 shows a small cycle interval, but large elements are shown to render a saw-tooth pattern [27] because of large increments.

5.6 Validating load conditions

To see if the boundary conditions are correctly set up, the stresses should be matched with expectations. In Figure 37 the stress distribution for the VCCT models is shown by S22 for DCB and S11 for ENF. In the DCB test, the stresses are mainly tensile normal to the interface and for the ENF test, the stresses are mainly shear.

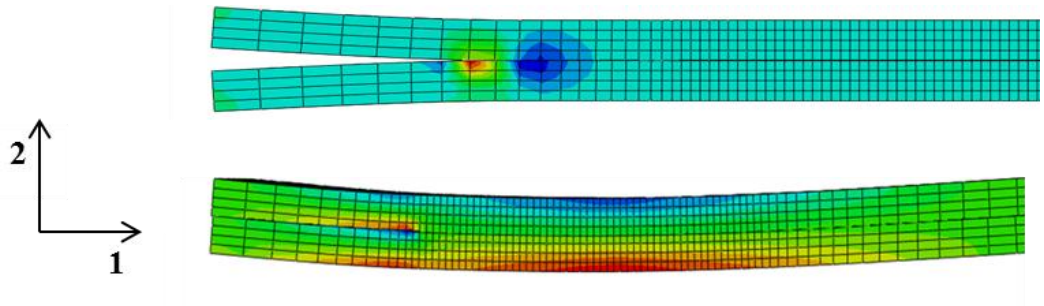

Figure 37 Stress distribution profiles, S22 for DCB (above) and S11 for ENF (below)

5.7 Compliance comparison

In VCCT, no compliance may be added due to lower stiffness of the adhesive layers. The effect of this will be higher stiffness than the test specimens and a resulting higher load when using the same energy release rate, as seen in Figure 38

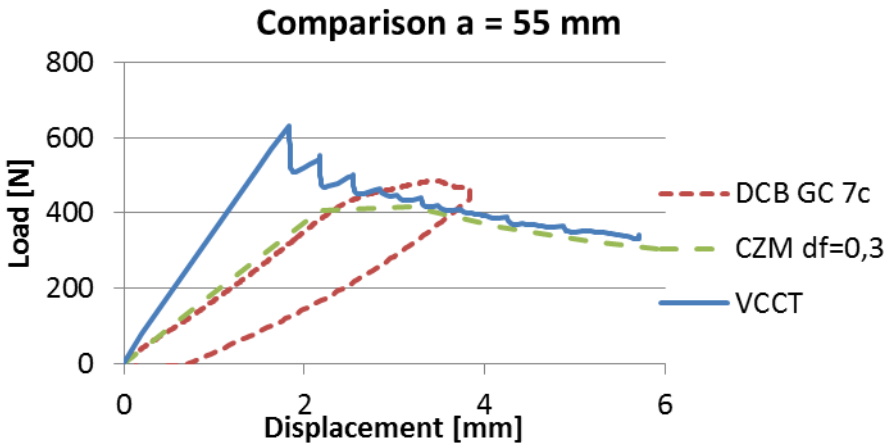

Figure 38: Comparison of CZM and VCCT

The CZM was modeled after procedure explained in the related project [9] and appendix B.2. A similar difference was seen for the ENF-model, shown in B.2.To understand how the error in compliance evolves with different crack lengths, a compliance curve was created for the DCB model. The model was loaded at different crack lengths ranging from 25 – 145 mm. It showed a lower compliance for smaller crack sizes, but an increase with longer cracks.

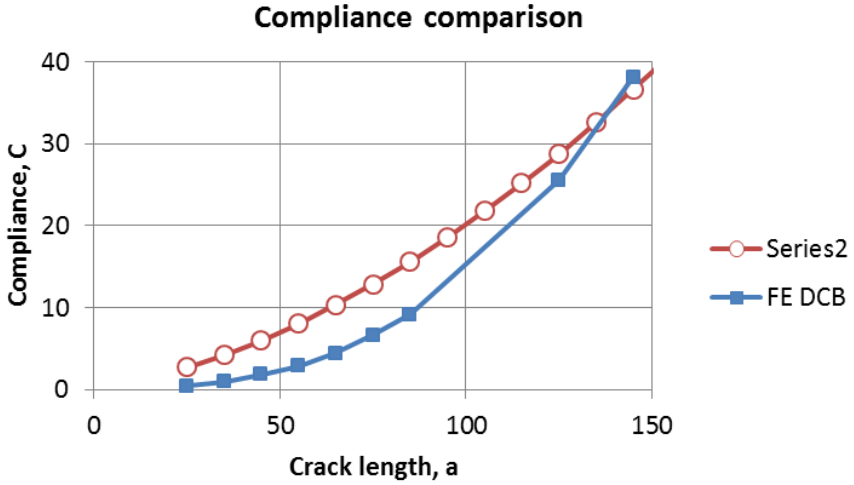

Figure 39: FE compliance, DCB

The same test was done for the ENF model. It was loaded at crack lengths 22 – 52 and fitted to equation (1.9). The resulting parameters are listed in A.5.

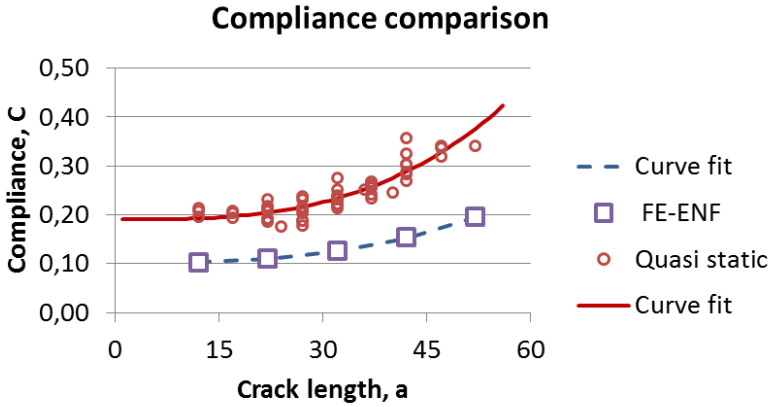

Figure 40: FE compliance, ENF

The compliance is generally lower also for the ENF model, and it also shows a lower increase with crack length.

5.8 Fatigue validation

Because the stiffness of the FE-model deviates from the tested specimens, the simulation may not be expected to yield similar response to the tested values and so the procedure must be validated separately. Following a procedure explained by Krueger [28], a benchmark example should be made for the crack initiation and propagation. First the δ_c and P_c is found by loading the model with the wanted crack length to crack propagation occurs. G_{IC} is verified and the values extracted. The δ_{max} is found by using the relation

$$\frac{\delta_{max}^{\ 2}}{\delta_c^{\ 2}} = \frac{G_{max}}{G_C} \tag{1.18}$$

The presumed crack onset N_a is found by the equation (1.5) and the number of cycles needed for degradation of one element is found by integrating (1.16)

$$\int dN = \int \frac{1}{C_3 \Delta G^{C_4}} da \tag{1.19}$$

Which, when integrated over one increment size, Δa, becomes

$$\Delta N = \frac{\Delta a}{C_3 \Delta G^{C_4}} \tag{1.20}$$

Here, the crack propagation increment size, Δa, is determined by the element size in the cohesive zone and ΔN is the number of cycles needed to propagate the crack front by one element. For an initial crack length a_0 of 37 mm the δ_c is found to be 0.86 mm. For a G_{max} of 209 J/m^2 and R=0.2, similar to the DCB GC C 6a specimen, this gives a $\delta_{mean} \pm \delta_{amp}$ = 0.2417 ± 0.1611 mm. The calculated number of cycles before onset then becomes N_a = 1420 cycles and the crack should propagate at 2000 cycles/mm.

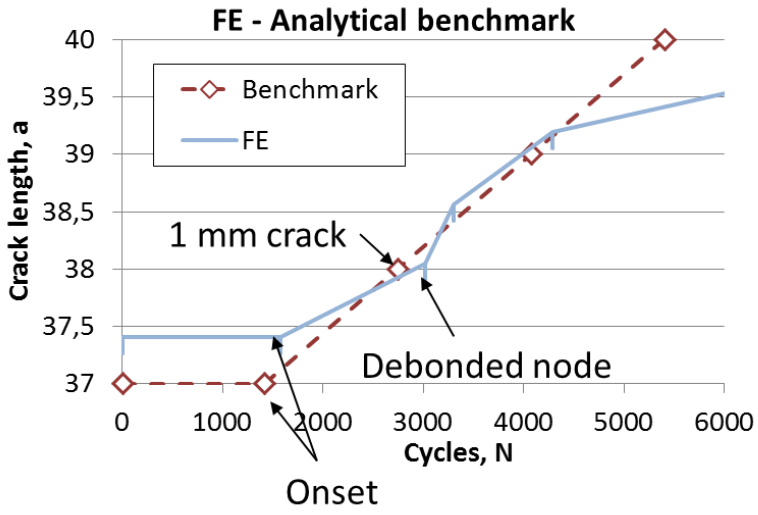

Figure 41: Benchmark against analytical procedure

We see a good correlation between the analytical and numerical calculation. A constant initial difference is noticed and the numerical model calculates an earlier onset. Only onset and first crack increment was calculated for benchmark and may be compared. The subsequent points are only linearly plotted as indications, and are not correct representations as the ΔG should decrease with crack evolution as seen with the FE-model. This is an example of the advantage of the numerical model.

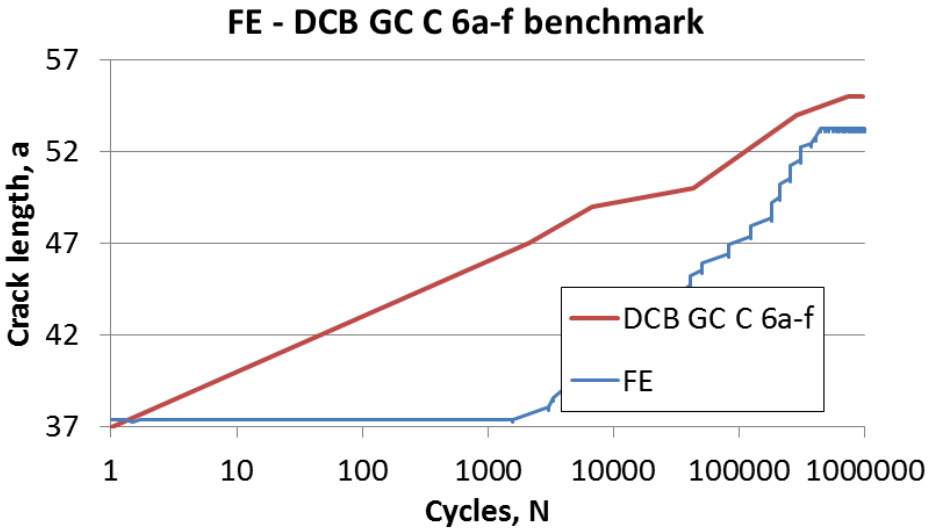

Figure 42: Benchmark against test specimen

Comparing with the specimen tested at equal ΔG, the FE model shows a slower initial propagation, but ends up at a similar crack length when approaching 10E6 cycles. At a crack length of 52.2 mm, the energy release rate in the model is lower than threshold value and it goes to a run out.

6 Discussion

6.1 Experimental

6.1.1 Crack measurement

The visual sighting of the crack front is problematic. A noted crack length spotted from the side of the specimens may differ greatly from crack front along the thickness direction. The suggested method to calculate the crack length became problematic when the compliance of the fatigue specimens was lower than the lowest compliance recorded in monotonic loading. The problem was especially apparent in the load controlled ENF specimens. A 50 kN load cell was used, and it could be that the measurements were incorrect on the account of noise. The same was done for DCB tests, but it being opening mode, the cracks could successfully be measured visually.

6.1.2 Load and displacement control

Load control and displacement control was tested. The standard recommends displacement control for stable crack growth, and this is critical if increased delamination is to be measured visually. Once onset is reached in load control, the crack grows exponentially faster. An issue noticed with the displacement control was the R-ratio, $\frac{\delta_{min}}{\delta_{max}}$. R < 0.1 does not insure that the specimen is always in loading. Due to mechanics of material relaxation this could lead to specimens cycling between load and fully relaxed position, $\frac{P_{min}}{P_{max}} \leq 0$. These are cases which are irrelevant for crack propagation, as crack will not grow under compression. Furthermore, the relaxation may induce unwanted effects at the point where the system changes state from static equilibrium to dynamic load condition and vice versa.

The suggested calculation of displacement limits for amplitude through $\frac{\delta_{\mathrm{max}}^2}{[\delta_{\mathrm{cr}}]_{\mathrm{av}}^2} = \frac{\mathrm{G_{max}}}{\mathrm{G_{cavg}}}$ did not prove consistent with the actually measured rates. A full backward calculation was used instead. Because data acquisition and machine control sensors were separate, small deviations between wanted and acquired energy release rates were present throughout testing.

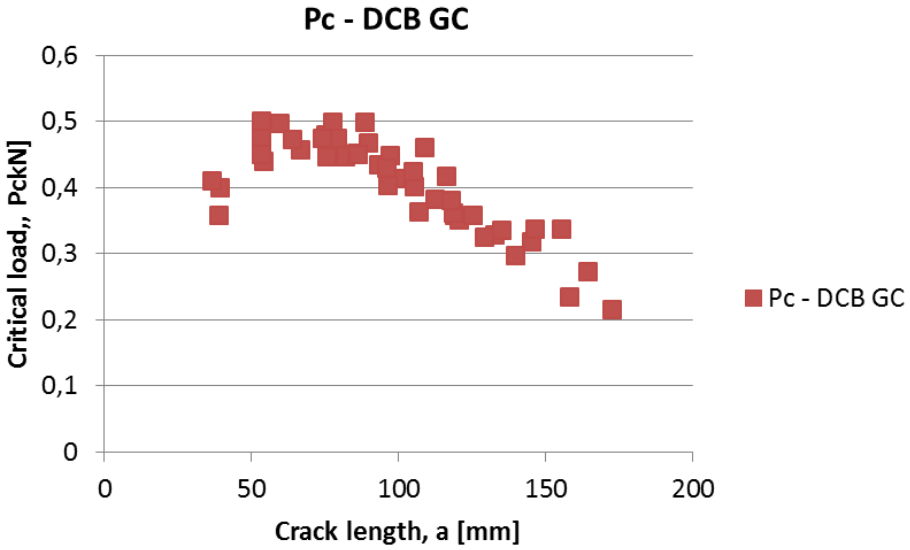

Figure 43: Critical load decreases with crack length

Friction was neglected for ENF in quasi static tests as it was shown to only yield a 2-4% overestimation of critical energy release rate. [23] However, in fatigue loading this could be of more importance and should be studied. In addition to hindering crack propagation, it could also generate heat in testing at higher frequencies.

6.2 Results validation

6.2.1 DCB tests

The DCB tests show relatively small scatter compared to the ENF tests. The crack front was less problematic to determine visually, and with displacement control, several increments were possible to do on each specimen. One issue may be the possible added compliance due to hinge application. This is discussed further in 6.3 Simulation.

6.2.2 ENF tests

ENF tests show a significant scatter compared to the DCB tests. Several indications of error have been noticed during testing:

- Compliance inconsistent with quasi-static tests
- Creep, or stress relaxation
- Crack measurement difficulties
- Large dimension load cell

The compliances of some fatigue specimens were lower than the ones measured during quasi-static tests. The test for strain rate dependency showed little to no change with increasing displacement rates of up to 60 mm/min. The load interval used for acquisition showed to have an effect. However, when accounted for in the fatigue tests, the compliances were still lower. A problem could be noise from the 50kN load cell. The relaxation was, if assumed present in the cyclic loading, only seen for the displacement controlled tests. The load controlled tests showed an opposite reaction as compliance decreased initially. The ambiguity makes it difficult to conclude, but is reasonable considering that the tested materials inherit different mechanical properties. One can also point at work hardening as a possible mechanism. At last there is the difficulty in finding a proper way of measuring crack length as described under 6.1.

6.2.3 Bridging

The bridging commented in 4.6 is thought to increase stiffness and create higher energy release rates. The effect will depend on the stiffness of the fibers and the specimen itself. The specimens tested had high stiffness compared to normal delamination tests on composites. In addition, the bridging fibers were of the glass fibers and not the UHM carbon fiber. One suggested method is to add a user-defined degradable cohesive element to simulate the fiber bridging in the crack zone [35]. Due to the reduced stiffness of these elements, this will interfere with the crack tip calculations in a VCCT analysis. Another suggested method by Spearing and Evans [36] is to calculate a new, larger arm thickness, h^*. This will add stiffness compensation to the model, increasing with leg length and with the benefit of not including more damage computation in the process zone

6.3 Simulation validation

6.3.1 Low cycle fatigue

The LCF-simulation is highly dependent on statistical data. It should work for different modes, mode mix and multi-axial/directional fatigue, however, it assumes the same power law crack propagation rate for all cases, only reducing and increasing the critical release rates based on mixed modes.

In Figure 41 the analysis shows a later onset for the numerical analysis than the benchmark value calculated in advance. The initial constant difference could be explained by the compliance calibration method used to determine the crack in the FE-model, given that, initially, the crack is well defined as 37 mm on the model, yet the calculated initial crack length reads 37.5 mm.

In Figure 42 the crack propagation rate of the FE-model is slower than the test specimen, which could be explained by special conditions of the tested specimen at the initial crack increment. As shown in Figure 43, the quasi-static tests done previously [9] showed lower critical loads for propagation increments starting from the insert. A similar effect is possible in this specimen. The simulation model reaches threshold value before it reaches the final crack length of the test specimen. This should be accounted for by reducing the threshold value. Krueger [27] suggests a value lower than the measured threshold due to composites fatigue behavior, and uses 0.06 in his benchmarking.

6.3.2 Compliance difference

When validated, both ENF and DCB models showed a higher stiffness than the experimental specimens. This becomes problematic when doing simulations, as different load conditions apply to achieve the same energy release rates, ie.: displacements from tests yield much smaller loads in the numerical models. This could be due to several reasons:

- Added compliance through setup
- Added compliance through adhesive interface
- Error in material parameters

- Error in data acquisition

The DCB had moving parts, and even though the piano hinges were enforced with thicker steel plates, the occurrence of compliance increase through the setup is probable. Compensation could be made by adding the compliant components to the simulation. The calculation of, and implementation of this, was not conducted. The three-point bending components were all in solid, thick steel, and may be considered rigid in the ENF setup.

One reason could be that with surface bonding there is no compliance added from the adhesive interface, and as such, a more rigid reaction is to be expected. There should be rotations and strains in the cohesive zone adding to the compliance. As shown in [9] altering the stiffness in the cohesive elements in CZM was able to compensate for the high stiffness in the model. For VCCT reducing the stiffness of elements near the cohesive zone could be a possibility, but this must be done without interfering with the VCCT fracture criterion. In addition, care should be taken not to compensate for the compliance added from other sources, as the final model would again be faulty if used on other geometries. The same argument is valid for using cohesive elements. Before changing the stiffness of the cohesive elements, other sources for compliance should be analyzed.

The material parameters selected for the simulation are not exact. The values for the carbon fiber composite were taken from tests conducted on a composite made of Pyrofil HS40 fibers which have a slightly higher elastic modulus than the Toray M46JB fibers used in production of the current tests. The same SE84LV resin system was used, but including a difference in volume fraction, could lead to a significant compliance difference.

Finally, an error in data acquisition is possible. The data from the DCB tests are consistent with the ones obtained during quasi-static tests done on a separate machine and data acquisition system earlier. The ENF tests were done using a 50kN load cell, tested loads did not exceed 5kN, which is recommended in the standard [5]. The specimens could have been influenced by the margin of error in the load estimation.

7 Conclusion

The aim of this thesis was to investigate the fatigue properties of the adhesive interface between steel and a composite reinforcement patch using tests and finite element method simulations. This was done through fatigue tests for fracture modes I and II and by finding a direct cyclic fatigue simulation.

Displacement controlled tests for DCB showed good consistency in results and many increments for each specimen was possible. Because ΔG decreases, a series of different ΔG may be tested for each specimen. The constants for crack onset were found to be C_1 = 0.840 and C_2 = -4.755 and the constants for crack propagation were found to be C_3 = 0.372 and C_4=3.972. The longest cycle life recorded was 4.35E5 cycles at 104 J/m^2 for Mode I and

The ENF specimens proved more complicated as the crack lengths were difficult to measure. Trying both calculating the crack length, as well as finding it by handheld microscope, the final solution was to use the known initial crack, and if there was ambiguity between load curve and crack front, the specimen was loaded until fracture for a new fatigue test increment. The constants for crack onset were found to be C_1 = 0.736 and C_2 = -5.945. The longest cycle life was 1.23E5 cycles at 122 J/m^2 for Mode II.

A simulation procedure was proposed for fatigue delamination using direct cyclic fatigue analysis and VCCT. The model displayed higher stiffness and because of this, the test input would render different behavior in the model, and different energy release rates would be present. Despite the difference in stiffness, the procedure itself was validated as a possible method for estimating crack propagation.

8 Further work

Due to the geometries tested and the purpose of this thesis, the mixed mode behavior has not been of significant importance. Tests plotting the mixed mode effect in G_{total} should be conducted to verify this before use on repairs containing probability of mixed mode load conditions. In addition, because of the unusual results that quasi-static tests show lower fracture resistance for Mode II than Mode I, an effort should be made to map and compare the behavior in Mode III conditions.

A way of determining the exact crack front should be found and used in further testing. Technologies devised for crack discovery of large structures should be tested for use in finding delamination of repair patches.

A nonlinear fatigue delamination method could yield better approximations considering the problems of fiber bridging and the nonlinear load response of epoxy.

In the search for a long term simulation, it could also be beneficial to further investigate the effects of the time deteriorating effects of the patch, such as creep.

For faster simulations, continuum shell element may be selected. In a benchmark analysis by Krueger [27] the use of continuum shell elements showed a reduction in computational effort reduced by a factor of 2.5 compared to the 3D solid elements.

9 Bibliography

[1] "Adhesives.org," Adhesives and Sealant Council, [Online]. Available: http://www.adhesives.org/TrainingEducation/StudentResources/DesignofAdhesiveBonds/MechanicsofAdhesion.aspx. [Accessed 20 November 2011].

[2] A. P. D.A. Dillard, Adhesion science and engineering, Elsevier Science Publishers, 2002.

[3] A. Griffith, "The Phenomena of Rupture and Flow in Solids," JSTOR, 1921.

[4] L. A. Carlsson and R. B. Pipes, "Experimental Characterization of Advanced Composite Materials," Prentice-Hall, Inc., 1987.

[5] ASTM International, "Standard Test Method for Mode I Fatigue Delamination Growth Onset of Unidirectional Fiber-Reinforced Polymer Matrix Composites," 2004.

[6] A. Kinloch and R. Young, "Fracture Behaviour of Polymers," Elsevier, 1983.

[7] ASTM International, "E739 Practice for Statistical Analysis of Linear or Linearied Stress-Life (S-N) and Strain-Life (e-N) Fatigue Data," 2010.

[8] P. Paris, M. Gomez and W. Anderson, A rational analytic theory of fatigue, 1961.

[9] A. Log, "Adhesion of metal-composite joints, European Co-Patch Project," NTNU, 2011.

[10] J. P. Berry, "Determination of Fracture Surface Energies by the Cleavage Technique," *Jornal of Applied Physics,* vol. 34, p. 62, 1963.

[11] M. L. Benzeggagh and M. Kenane, "Measurement of mixed-mode delamination fracture toughness of unidirectional glass/epoxy composites with mixed-mode bending apparatus," *Composites Science and Technology,* vol. 56, pp. 439-449, 1996.

[12] ASTM International, "Standard Test Method for Mode I Interlaminar Fracture Toughness of Unidirectional Fiber-Reinforced Polymer Matrix Composites," 2007.

[13] K. Shivakumar, H. Chen and S. A. Smith, "An Evaluation of Data Reduction Methods for Opening Mode Fracture Toughness of Sandwich Panels," *Journal of Sandwich Structures and Materials,* vol. 7, p. 77, 2005.

[14] H. W. Andresen and A. T. Echtermeyer, "Critical energy release rate fr a a CSM reinforced carbon fibre composite/steel bonding," Elsevier, 2005.

[15] A. Sinnerud, "Adhesion of metal-composite joints," NTNU, 2011.

[16] B. D. Davidson and S. S. Teller, "Recommendations for an ASTM Standardized Test for Determining GIIc of Unidirectional Laminated Polymeric Matrix Composites," ASTM International, 2010.

[17] J. Li, K. O'Brien and S. M. Lee, "Comparison of Mode II and III monotonic and fatigue delamination onset behavior for carbon composites," National Research Council, NASA, Hampton, VA.

[18] A. Russel and K. Street, “Factors affecting the interlaminar fracture of graphite/epoxy laminate,” 1982.

[19] N. Standard, “M-501 Surface preparation and protective coating,” www.standard.no, 2004.

[20] “ISO 8501 Preperation of steel substrates before application of paints and related products,” International Standard Organization, 1996.

[21] “ISO 8503 Preperation of steel substrates before application of paints and related products,” Internation Standards Organization, 1996.

[22] “SE 84LV - Low Temp Epoxy Prepreg System (v12),” SP Gurit, 2010.

[23] Gillespie, Carlsson, Pipes, Rotshcilds, Trethewey and Smiley, “Delamination growth in composite materials,” Center for composite materials, University of Delaware.

[24] D. L. Erdman and J. M. Starbuck, “Fatigue crack growth in adhesive joints,” Oak Ridge National Laboratory.

[25] A. Pirondi and G. Nicoletto, “Fatigue crack growth in bonded DCB specimens,” Elsevier, 2004.

[26] A. J. Vinciquerra and B. D. Davidson, “Effect of Crack Length Measurement Technique and Data,” *Journal of Reinforced Plastics and Composites,* p. pp. 1051–1062., 2004.

[27] K. Song, C. Dávila and C. A. Rose, “Guidelines and Parameter Selection for the Simulation of Progressive Delamination,” SIMULIA, 2008.

[28] R. Krueger, “Development of a Benchmark Example for Delamination Fatigue Growth Prediction,” NASA, Hampton, 2010.

[29] Simulia Corp., Abaqus Analysis User's Manual - Low-cycle fatigue analysis using the direct cyclic approach.

[30] M. Kenane and M. L. Benzeggagh, “Mixed-mode delamination fracture toughness of unidirectional glass/epoxy composites,” *Composites Science and Technology*, vol. 57, pp. 597-605, 1997.

[31] Momentive, “EPIKOTE Resin MGS RIMR 135 and EPIKURE Curing Agent MGS RIMH 134–RIMH 137,” 2006.

[32] A. Sinnerud, “Adhesion of metal-composite joints,” 2010.

[33] ASTM International, “E8 / E8M - 09 Standard Test Methods for Tension Testing of Metallic Materials,” 2012.

[34] R. Krueger, “Approach to Assess Delamination Propagation Simulation Capabilities in Commercial Finite Element Codes,” NASA, Hampton, 2008.

[35] S. Feih, “Development of a user element in ABAQUS for modellingof cohesive laws in composite structures,” Risø-Report, Roskilde, 2005.

[36] S. M. Spearing and A. G. Evans, “The role of fiber bridging in the delamination resistance of fiber-reinforced composites,” *Acta metall. mater.,* vol. 40, no. 9, pp. 2191-2199, 1992.

[37] T. Diehl, “Using ABAQUS Cohesive Elements to Model Peeling of an Epoxy-bonded Aluminum Strip: A Benchmark Study for Inelastic Peel Arms,” in *2006 ABAQUS Users' Conference*, 2006.

[38] T. Diehl, “On using a penalty-based cohesive-zone finite element approach, Part I: Elastic solution benchmarks,” International Journal of Adhesion and Adhesives, 2007.

[39] G. S. S. Lâaszlâo P. Kollâar, Mechanics of Composite Structures, Cambridge University Press, 2003.

[40] D. Roylance, “Introduction to Fracture Mechanics,” Massachusetts Institute of Technology, Cambrigde, MA, 2001.

[41] Y. O. S. T. Toshio Nagashima, “Stress intensity factor analysis of interface cracks using X-FEM,” John Wiley & Sons, 2003.

[42] Sun, B. D. Davidson and Xuekun, “Geometry and Data Reduction Recommendations for a Standardized End Notch Flexure Test for Unidirectional Composites,” ASTM International, 2006.

[43] Y. J. Prel, P. Davies, M. L. Benzeggagh and F.-X. de Charantenay, “Mode I and Mode II Delamination of Thermosetting and Thermoplastic Composites,” *Composite Materials: Fatigue and Fracture, Second Volume,* vol. Second, pp. 251-269, 1989.

[44] C. L.F., “A study of the effects of cyclic thermal stresses on a ductile metal,” *Trans. ASME,* vol. 76, 1954.

[45] Simulia Corp., “Selecting Material Parameters for Cohesive Elements Defined in Terms of Traction-Seperation”.

A.1 Matlab script

```
function compliancefatigue(data)
data(:,3)=data(:,3)-data(1,3);
c=[0,0];
k=1;
l=1;
comp=[0,0,0];
length=numel(data(:,2));
for i = 1:length-1
    c=0;
    if data(i+1,2) > data(i,2) & 0.1<data(i,2)
        comp(l,:) = data(i,:);
        l = l+1;
    end

    if data(i+1,2) < data(i,2) & comp(:,1)>0
        if numel(comp(:,2))<2
            c=c;
        else
            c=polyfit(comp(:,2),comp(:,3),1);
        end

        ccurve(k,2)=c(1,1);
        ccurve(k,1)=data(i,1);
        comp=[0,0,0];
        l=1;
        k=k+1;
    end
end
subplot(3,1,1); plot(data(:,1),data(:,2));
title(inputname(1))
legend('Load curve','Location','NorthEast')
xlabel('Time, t [s]')
ylabel('Load, P [kN]')
subplot(3,1,2); plot(data(:,1),data(:,3));
legend('Displacement
curve','Location','NorthEast')
xlabel('Time, t [s]')
ylabel('Displacement, /Delta [mm]')
subplot(3,1,3); plot(ccurve(:,1),ccurve(:,2));
legend('Compliance curve','Location','NorthEast')
xlabel('Time, t [s]')
ylabel('Compliance, C [mm/kN]')
```

Calculate compliance during fatigue testing.

Zero the displacement.

If load is increasing, record data.

If load has stopped increasing, stop recording and make a linearization.

Insert linear fit into curve.

Plot load curve, displacement curve and compliance curve.

A.2 Specimen production

A list of specimens produced for the project report [9]. Abbreviations were used for reference. N is for Needle gun surface preparation. G is for grit blasted surface preparation. C is for pre-cured glass fiber layer. P is for pre-impregnated glass fiber layer, The tests in bold are the ones conducted for this thesis.

Table 5: Full batch of specimens produced

	Precured glass fibre	Pre-preg glass fibre
Needle gun	8x ENF-NC	8x ENF-NP
Grit blasted	8x ENF-GC, **8x ENF-GC-C**	8x ENF-GP

	Precured glass fibre	Pre-preg glass fibre
Needle gun	8x DCB-NC	8x DCB-NP
Grit blasted	8x DCB-GC, **8x DCB-GC-C**	8x DCB-GP

A.3 Quasi-static tests, DCB

Using the relation (1.7) the average G_{IC} was calculated and a function C (a) found.

Table 6: DCB quasi static tests

Specimen	Cycle	Compliance C [mm/kN]	Crack length, a [mm]	GIC [J/m^2]
7	a	4,67	39,0	529,2
	b	5,53	54,3	682,1
	c	7,15	66,8	776,2
	d	8,74	75,8	798,8
	e	10,31	82,0	866,2
	f	11,20	86,0	919,0
	g	13,34	93,3	934,4
	h	15,36	99,3	912,6
	i	17,50	105,3	929,8
	j	19,77	112,3	895,0
	k	22,43	119,3	836,1
6	a	6,23	39,5	882,2
	b	7,37	59,8	1061,9
	c	9,68	75,3	1033,7
	d	13,51	89,8	1143,9
	e	17,34	105,0	1039,5
	f	25,86	120,5	919,2
	g	33,03	132,8	938,2
	h	44,85	145,3	1094,5
	i	63,35	164,5	1005,5
4	a	6,12	53,5	897,3
	b	7,98	77,5	890,6
	c	11,02	88,5	1077,6
	d	13,18	97,3	952,2
	e	17,18	109,0	1165,4
	f	19,66	116,3	1028,9
	g	24,75	125,5	877,8
	h	30,19	135,0	880,7
	i	36,53	146,5	993,6
	j	45,15	155,5	1157,0

Specimen	Cycle	Compliance C [mm/kN]	Crack length, a [mm]	GIC [J/m^2]
3	a	4,65	36,8	741,2
	b	7,09	53,5	1158,7
	c	7,97	64,0	967,4
	d	10,19	79,0	1012,6
	e	12,95	96,0	866,5
	f	21,21	118,5	817,9
	g	35,94	139,8	796,7
	h	49,12	158,0	599,9
	i	70,65	172,8	665,6
2	a	4,54	53,5	706,0
	b	7,45	74,3	919,1
	c	10,13	86,3	976,8
	d	11,38	96,5	802,7
	e	16,64	107,0	869,5
	f	20,51	118,0	927,1
	g	26,79	129,3	950,4
Average				910,8
Std. Dev				142,6

A.4 Quasi-static tests, ENF

Specimen	#	Crack length, a [mm]	GIC [J/m^2]	Critical load, Pc [kN]
1	a	36	825,15	2,845
	b	32	591,90	2,795
	c	27	805,04	4,127
	d	24	673,30	4,2
2	a	32	387,71	2,17
	b	40	717,09	2,52
3	a	22	508,72	3,562
	b	22	582,77	3,66
	c	22	767,16	4,618
	d	22	868,51	4,92
4	a	27	564,09	3,154
	b	27	933,76	4,306
	c	27	1017,37	4,515
	d	27	1354,51	4,993
5	a	32	724,92	3,08
	b	32	807,96	3,25
	c	32	880,87	3,45
	d	32	1020,17	3,54
6	a	37	477,73	2,06
	b	37	622,86	2,41
	c	37	706,08	2,68
	d	37	694,73	2,62
7	a	42	501,94	1,86
	b	42	710,99	2,13
	c	42	1482,13	2,93
Average			769,10	3,29

Specimen	Cycle	Crack length, a [mm]	Complaince, C [mm/kN]
1	a	12	0,2085
	b	17	0,2072
	c	22	0,1851
	d	27	0,2154
	e	32	0,235
	f	37	0,2581
	g	42	0,2877
	h	47	0,3202
	i	36	0,2516
	j	32	0,2194
	k	27	0,178
	l	24	0,1754
2	a	12	0,1968
	b	17	0,203
	c	22	0,2179
	d	27	0,238
	e	32	0,2524
	f	37	0,2592
	g	42	0,269
	h	47	0,3366
	i	32	0,2393
	j	40	0,2463
3	a	12	0,2138
	b	22	0,214
	c	32	0,2749
	d	22	0,214
	e	22	0,2322
	f	22	0,192
	g	22	0,1915
4	a	17	0,1942
	b	27	0,2127
	c	37	0,261
	d	27	0,2127
	e	27	0,1889
	f	27	0,1872
	g	27	0,2038

Specimen	Cycle	Crack length, a [mm]	Compliance, C [mm/kN]
5	a	22	0,2081
	b	32	0,222
	c	42	0,2829
	d	32	0,222
	e	32	0,2215
	f	32	0,2148
	g	32	0,2364
6	a	27	0,2313
	b	37	0,2667
	c	47	0,3407
	d	37	0,2667
	e	37	0,2548
	f	37	0,2334
	g	37	0,2412
7	a	32	0,2313
	b	42	0,3026
	c	52	0,3407
	d	42	0,3026
	e	42	0,3254
	f	42	0,3579

A.5 Compliance calibrations

Table 7: DCB compliance, quasi-static

Parameter	Value	StdErr	CV(%)
h	-2,26	0,17	7,53
n	1,74	0,09	4,94

Table 8: ENF compliance, quasi-static

Parameter	Value	StdErr	CV(%)
α	1,90E-01	4,27E-03	2,24E+00
β	1,32E-06	8,73E-08	6,59E+00

Table 9: DCB compliance, FE

Parameter	Value	StdErr	CV(%)
h	-3,95E+00	7,00E-02	1,77E+00
n	2,55E+00	3,85E-02	1,51E+00

Table 10: ENF compliance, FE

Parameter	Value	StdErr	CV(%)
α	1,03E-01	7,33E-04	7,10E-01
β	6,58E-07	1,01E-08	1,53E+00

A.6 Fatigue data, DCB tests

#	Pmin	Pmax	da/dN	ΔG	Na	Gmax	f
2e	0,103	0,416	9,05E-03	386	221	398	1 Hz
2f	0,090	0,388	2,62E-03	338	855	347	1 Hz
2g	0,077	0,375	3,43E-03	288	550	294	1 Hz
2i	0,064	0,359	2,67E-03	269	785	274	1 Hz
2j	0,063	0,375	1,51E-03	287	443	292	1 Hz
2k	0,058	0,350	2,92E-03	269	949	274	1 Hz
2m	0,033	0,324	1,06E-03	347	1222	351	1 Hz
2n	0,041	0,335	1,64E-03	369	735	374	1 Hz
2o	0,061	0,392	2,70E-02	470	74	478	1 Hz
2p	0,054	0,381	7,54E-03	461	311	467	1 Hz
2q	0,049	0,384	7,73E-03	500	181	506	1 Hz
2r	0,042	0,363	3,53E-03	476	243	481	1 Hz
2s	0,039	0,350	4,26E-03	476	302	482	1 Hz
2t	0,036	0,346	7,69E-03	494	134	499	1 Hz
2u	0,039	0,342	2,01E-02	506	30	512	1 Hz
2v	0,035	0,355	1,43E-02	548	78	554	1 Hz
2w	0,029	0,352	2,88E-02	567	113	571	1 Hz
2x	0,027	0,360	3,49E-02	607	56	612	1 Hz
2y	0,026	0,364	1,65E-02	633	53	637	1 Hz
2z	0,023	0,349	1,46E-02	619	96	623	1 Hz
2aa	0,028	0,353	2,90E-02	649	63	654	1 Hz
2ab	0,026	0,344	1,12E-02	645	63	650	1 Hz
2ac	0,024	0,320	3,05E-02	591	20	596	1 Hz
2ad	0,023	0,318	1,02E-02	608	53	612	1 Hz
2ae	0,019	0,290	3,70E-02	580	138	584	1 Hz
2af	0,017	0,296	3,26E-02	513	48	516	1 Hz
2ag	0,016	0,289	1,26E-02	610	81	614	1 Hz
2ah	0,014	0,267	1,89E-02	572	149	575	1 Hz
2ai	0,011	0,257	1,08E-02	560	128	562	1 Hz

#	Pmin	Pmax	da/dN	ΔG	Na	Gmax	f
3b	0,037	0,280	9,90E-04	188	2021	192	1 Hz
3c	0,055	0,267	9,01E-03	176	444	181	1 Hz
3d	0,017	0,441	2,00E+01	559	1	561	1 Hz
3e	0,018	0,393	1,13E-01	172	62	174	1 Hz
3f	0,011	0,349	1,69E-02	291	237	292	1 Hz
3g	0,004	0,302	1,11E-02	334	452	334	1 Hz
3h	0,001	0,279	0,00E+00	287	222	287	1 Hz
3i	0,001	0,273	1,55E-03	282	1288	282	1 Hz
3j	0,001	0,244	4,03E-04	246	1697	246	1 Hz
3k	0,008	0,245	1,20E-03	246	2186	247	1 Hz
3l	0,001	0,207	4,08E-04	193	2450	194	1 Hz
3m	0,000	0,199	9,96E-05	182	5736	182	1 Hz
5a	0,050	0,417	2,90E+01	794	16	805	1 Hz
5b	0,039	0,381	2,28E-02	415	78	419	1 Hz
5c	0,055	0,294	1,78E-03	253	1684	264	1 Hz
5d	0,048	0,275	8,75E-04	228	3253	237	1 Hz
5e	0,062	0,195	2,32E-05	95	43160	95	4Hz
6a	0,084	0,288	4,64E-03	194	2156	210	4Hz
6b	0,088	0,276	4,39E-04	146	4560	160	4Hz
6c	0,065	0,259	2,80E-05	132	19440	141	4Hz
6d	0,041	0,229	1,63E-05	112	29044	117	4Hz
6e	0,018	0,1931	2,295E-06	105	435760	106	4Hz
6f	0,015	0,1849	2,649E-06	86	236000	88	4Hz

A.7 Fatigue data, ENF tests

#	Pmin	Pmax	a	N	ΔG	C
Load control						
1a	-2,28	-0,23	22	640	210,20	0,14
1a	-2,28	-0,23	22	2400	203,13	0,14
1b	-2,29	-0,23	22	7955	256,81	0,17
2a	-2,28	-0,23	32	182	786,61	0,32
2b	-2,47	-0,25	29	139	434,96	0,17
2c	-2,28	-0,23	27	2992	350,28	0,18
2c	-2,28	-0,23	47	500	628,30	0,19
3a	-1,77	-0,18	12	2499	47,07	0,18
3b	-1,76	-0,18	22	3999	145,12	0,17
3b	-1,76	-0,18	27	10000	220,63	0,17
3b	-1,76	-0,18	37	5000	419,86	0,17
3c	-1,77	-0,18	22	4580	163,84	0,19
4a	-2,64	-0,26	22	120	369,99	0,18
4b	-2,47	-0,25	22	450	286,98	0,16
5b	-1,33	-0,13	32	650	179,35	0,21
5b	-1,33	-0,13	43	600	242,25	0,21
5b	-1,33	-0,13	45	900	258,49	0,22
5b	-1,33	-0,13	55	1600	287,64	0,23
5b	-1,33	-0,13	61	2800	302,35	0,25
5c	-0,96	-0,10	32	15900	116,80	0,26
5c	-0,96	-0,10	32	123000	122,64	0,27
Displacement control						
6b	-1,73	0,00	22	7100	164,16	0,19
6b	-1,68	0,00	22	33800	165,80	0,20
7a	-1,75	0,00	22	40	199,45	0,22
7b	-1,28	0,00	22	26350	93,74	0,20
7b	-1,28	0,00	22	88000	99,59	0,21
7c	-0,95	0,00	22	1200	67,83	0,26
7c	-0,88	0,00	22	3500	61,34	0,27

A.8 Fatigue parameter, curve fit

To find the parameters from the GN curves, linear fits are found for the G vs N plots in logarithmic scale. The parameters are acquired starting with:

$$\log(\Delta G) = \mathrm{m}_2 \log(N) + m_1$$

$$C_1 = \frac{1}{10^{m_1}}$$

$$C_2 = \frac{1}{m_2}$$

Likewise for the da/dN-curve:

$$\log\left(\frac{da}{dN}\right) = m_4 \log(\Delta G) + m_3$$

$$C_3 = 10^{m_3}$$

$$C_4 = m_4$$

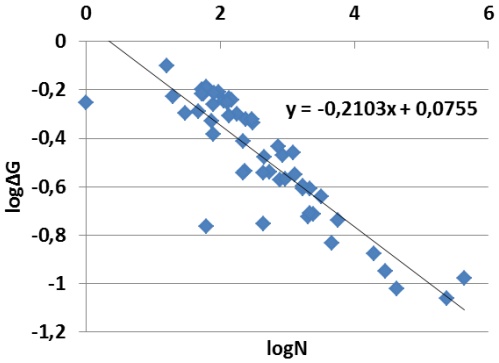

Figure 44: G-N curve fit, DCB

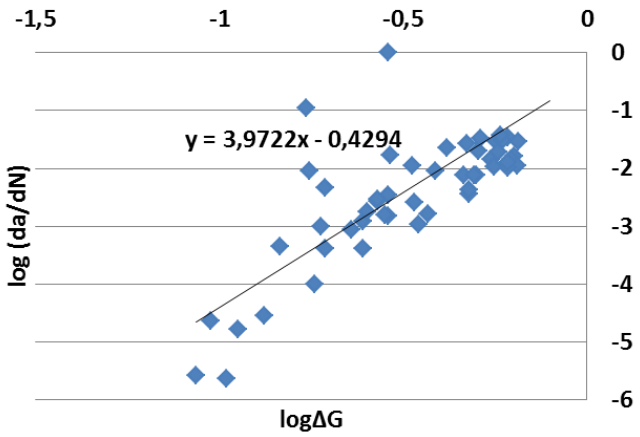

Figure 45: Crack propagation rate, curve fit, DCB

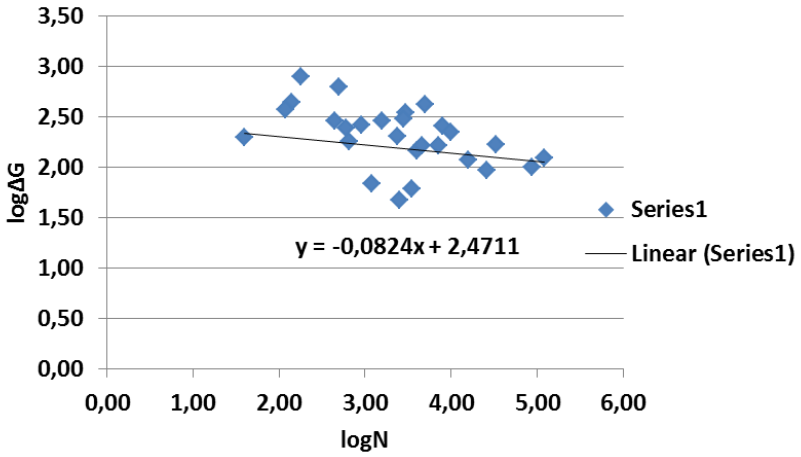

Figure 46: G-N curve fit, ENF

A.9 Fatigue parameters

Table 11: LCF Criterion Parameters, ENF

G-N constants, ENF	
C1	0,736
C2	-5,945

Table 12: LCF Criterion Parameters, DCB

G-N constants, DCB		**Paris' constants, DCB**	
C1	0,840	C3	0,372
C2	-4,755	C4	3,972

B. Simulation procedure

B.1 Simulation parameters

Table 13: LCF Criterion Parameters, DCB

G-N constants, DCB		Paris' constants, DCB	
C1	0,840	C3	0,372
C2	-4,755	C4	3,972

Table 14: Direct Cyclic Step Parameters

Direct cyclic step	**Fatigue**		
Cyce time period	1		
Max number of increments	100000		
Increment size	0,1		
Max number of iterations	5		
Number of fourier terms	Initial 25	Max 25	Increment 5
Cycle increment size	Min 10	Max 100	
Maximum number of cycles	100000		
Damage extrapolation tolerance	1		

Table 15: Amplitude Parameters

Parameters amplitude	
ω	6,28
A0	d_mean
A1	d_amp
t0	0

Table 16: VCCT Parameters

Parameters VCCT	
GIC	0,91
GIIC	0,769
GIIIC	0,769
η	2,284

B.2 Load curve comparison, ENF

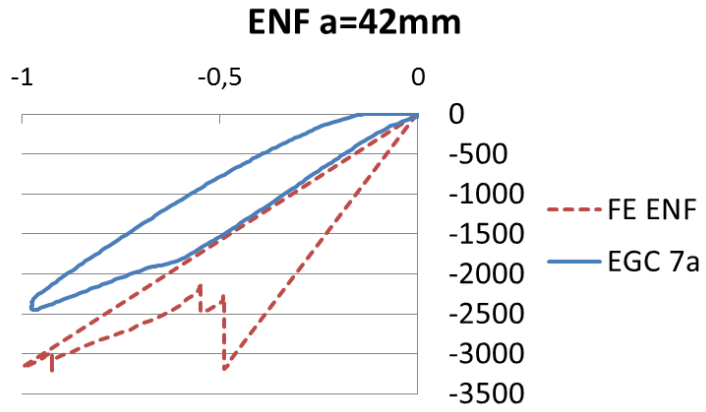

Figure 47: Load curves comparison of FE-model and a specimen of equal crack length

B.3 Cohesive Zone Modelling

A way of modelling crack propagation in a known direction such as adhesive interfaces or delamination, is cohesive zone modelling, CZM. This uses a set of cohesive elements, which are bonding elements between two surfaces of solid element instances. When the elements are strained, they lose stiffness by the formula

$$t_i = (1-d) K_i \delta_i \tag{1.21}$$

Here t_i is traction, d is the damage variable, which has the value d = 0 when the interface is undamaged, and the value d = 1 when the interface is fully fractured. Fully degraded elements are fully compliant and take up no forces in the structure in further increments. As elements are fully degraded, they are deleted so as to not cause slow simulations due to large time increment estimations as recommended by Diehl [37].

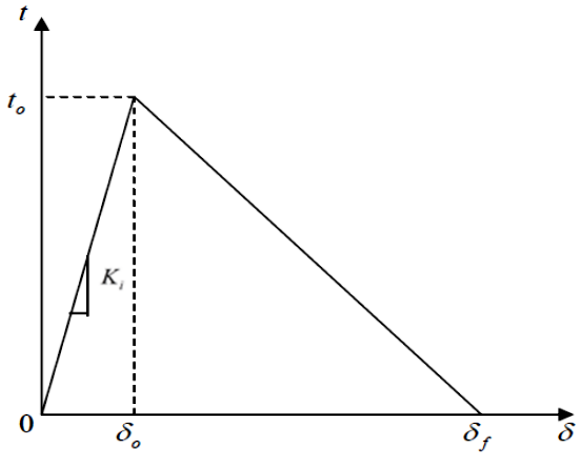

Figure 48: Traction-separation law

The controlling parameters for the critical strain, are the energy release rate, G_c, the interface strength $S_i$which is the maximum stress of the bond and the traction-separation relation [38]. Although data for the epoxy strength and stiffness are given by the supplier, the same values at the interface are likely to differ. A proposed way of calculating interface strength is

$$S_i = \frac{2G_i}{\delta_f} \tag{1.22}$$

The cohesive stiffness K_i is the individual stiffness of each element and was defined by Diehl as [38]

$$K_i = \frac{2G_i}{\delta_{ratio}(\delta_f)^2} \tag{1.23}$$

The total stiffness is dependent on the size of the elements. For the analysis used in chapter 5.7, an element size of 1 mm was used, a failure displacement of 0.3 and the stiffness and strength were adjusted accordingly. This model may only be used on other geometries provided that the same production method and bond thickness is attained.

C. Setup

C.1 Steel characterization tests

Tests were done using an Instron 100kN machine. The specimens were not machined and retained the geometries of 25 mm x 250 mm. Strain gauges were placed on the middle of each specimen. Specimens were loaded at a rate of 0.3mm/min for loads under 25kN. After 25kN, plasticity was certain and load rate was increased to 5mm/min until fracture occurred. For E-modulus, the specimens were loaded three times within elastic area.

Specimen	Width [mm]	Thickness [mm]	Cross-sectional area [mm^2]	Cycle	Modulus of Elasticity [MPa]			
					Extensometer		Strain gauge	
9TC	25,60	5,07	129,69	1	186 448		211 945	
				2	186 397		208 787	
				3	186 159		209 925	
14TP	26,02	5,04	131,14	1	184 223		200 918	
				2	184 068		201 443	
				3	183 494		198 494	
Mean Transverse					185 131	1 344	205 252	5 623
4LC	25,41	5,09	129,42	1	175 123		224 832	
				2	176 362		225 229	
				3	186 407		225 008	
16LP	25,90	5,02	129,93	1	209 153		206 439	
				2	181 905		216 648	
				3	179 057		216 912	
Mean Longitudinal					184 668	12 663	219 178	7 435

Table 17: E-modulus, steel tests

Position		Specimen	Width [mm]	Thickness [mm]	Cross-sectional area [mm^2]	Yield Strength [MPa]	Tensile strength [MPa]
Transverse	Center	1TC	25,34	5,08	128,64	389,80	443,79
		2TC	25,24	5,04	127,23	392,90	451,27
		10TC	25,24	5,03	126,96		
		Sub-mean	-	-	-	391,35	447,53
	Side	5TS	25,71	5,06	130,09	407,30	450,74
		6TS	25,18	5,08	127,85	395,90	444,62
		13TP	25,75	5,03	129,52	385,60	448,75
		Sub-mean	-	-	-	396,27	448,03
Longitudinal	Center	3LC	25,48	5,06	128,83	381,50	446,53
		4LC	25,41	5,09	129,42		
		11LC	25,28	5,08	128,41	377,20	448,37
		Sub-mean	-	-	-	379,35	447,45
	Side	7LS	25,18	5,06	127,41	394,20	463,29
		8LS	25,28	5,05	127,68	386,50	448,26
		15LP	25,78	5,01	129,06	385,50	450,99
		Sub-mean	-	-	-	388,73	454,18
Total						389,64	449,66

Table 18: Yield and tensile strength, steel tests

On 14TP and 16LP strain gauges were placed transverse of length direction to attain the Poisson's ratio by the formula $= -\frac{\varepsilon_2}{\varepsilon_1}$.

Poisson's ratio		
16LP	0,319	
	0,338	
	0,338	
Sub-mean	0,332	0,011
14TP	0,269	
	0,265	
	0,267	
Sub-mean	0,267	0,002
Mean	0,299	0,036

Table 19: Poisson's ratio, steel tests

C.2 Equipment calibration

Externally applied load cell and LVDT were calibrated and checked for linearity.

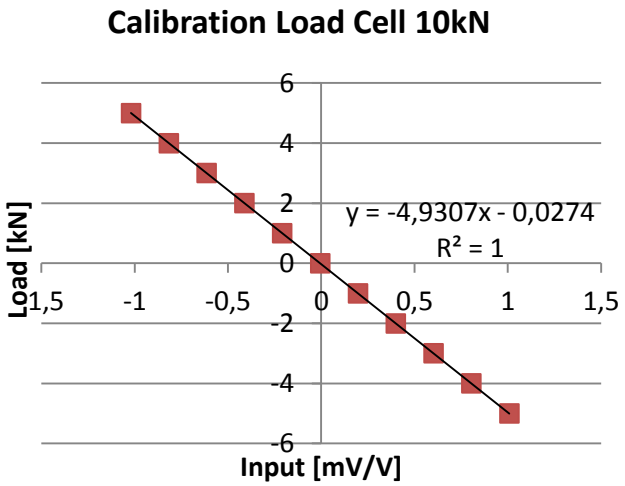

Calibration Load cell	
mv/V	kN
-1,0194	5
-0,81648	4
-0,6144	3
-0,41172	2
-0,20844	1
-0,00528	0
0,19816	-1
0,3996	-2
0,60264	-3
0,80532	-4
1,00896	-5

Figure 49: Calibration load cell

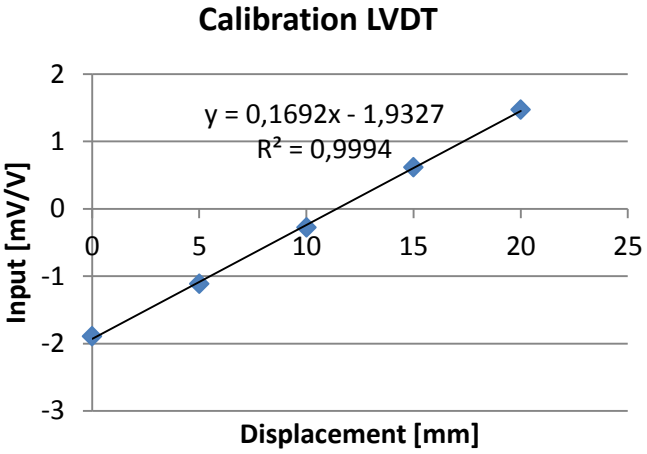

Calibration LVDT	
mv/V	Displ.
1,4712	20
0,6136	15
-0,28	10
-1,114	5
-1,8948	0

Figure 50: Calibration LVDT